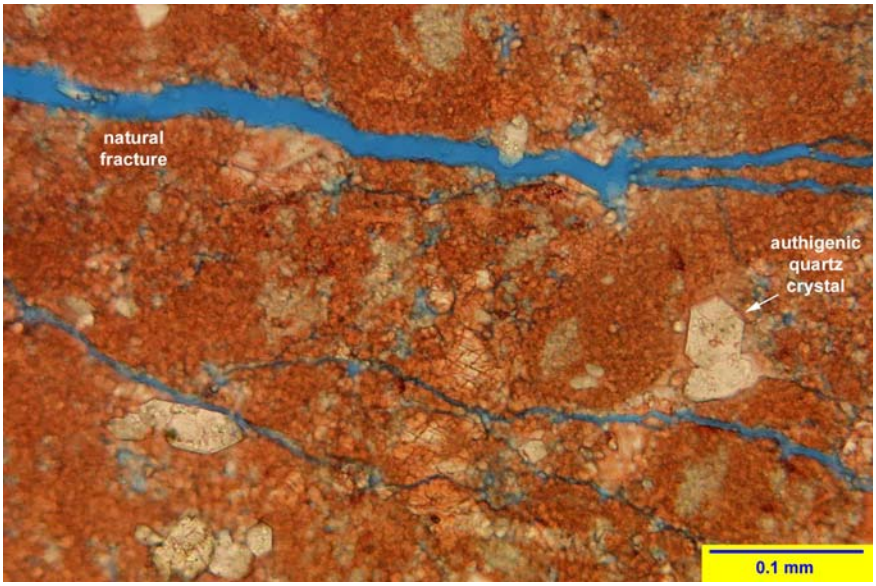

TOMBALL TECHNOLOGY CENTER

ANALYSIS OF WHOLECORE SEGMENTS

BIG LIME FORMATION
HARDY #14 WELL
CHARLESTON EAST FIELD
KANAHWA COUNTY, WEST VIRGINIA
API # 47-039-01997-0000

TECHNOLOGY CENTER REPORT NO. 06-10-0906

BJ SERVICES TECHNICAL REPRESENTATIVE
MR. ROGER MYERS
PITTSBURG, PA
DECEMBER 21, 2006

ANALYSIS OF WHOLECORE SEGMENTS

Table of Contents

EXECUTIVE SUMMARY:

Big Lime conventional wholecore segments obtained from the West Virginia Geological and Economic Survey were submitted to the Technical Services Group at the Tomball Technology Center for analysis. Multiple laboratories within Technical Services participated in the evaluation: this report details the findings of the Geological Services group. The objectives of this analysis were to characterize framework mineralogy, cements, clays, and porosity types present in the samples, and identify potential completion problems. Analyses conducted were stereomicroscopy, porosity and permeability measurement, acid solubility, insoluble residue analysis, thin section petrographic analysis, scanning electron microscopy/energy dispersive spectrometry (SEM/EDS), and X-ray diffraction (XRD).

Helium porosity and gas permeability values were determined on coreplugs drilled from the wholecore segments. A permeability versus porosity crossplot indicates that porosity and permeability in these samples generally has a log-normal relationship, i.e., permeability is controlled by interparticle porosity, rather than the typical carbonate "shotgun" patterns associated with various types of dissolution porosity. The log-normal relationship seen in these samples appears to be primarily the result of the original carbonate sand depositional environment, with some modification by the dolomitization process. Depth plots of the core analysis data revealed trends related to both depositional environments and the diagenetic processes that the carbonates have undergone during geologic time. In this well, grain density increases with depth, as a function of a) dolomitization, and b) decreasing amounts of quartz grains intermixed with the carbonate sand. The data further indicates that porosity is controlled both by the degree of dolomitization and the size of the detrital carbonate grains.

The mineralogical analysis indicates that the top few feet of the Big Lime are limestones, followed by several feet of calcareous dolomite, which overlies a clean dolomite section. Quartz is present in all samples, but increases significantly in the dolomitic sections to an average of 12.5%. Illite was the only clay noted by XRD techniques, and is present in only trace amounts.

Acid solubility of a sub-set of samples in 15% HCl averaged 90%. SEM examination of the insoluble residues revealed authigenic, hexagonal, euhedral quartz crystals in the upper limestone interval, and detrital quartz grains in the dolomitic section. The sand-sized detrital quartz grains are coated with roughly-textured authigenic quartz crystals on the grain surfaces. The authigenic quartz coating was precipitated from silica-rich formation waters, growing from nucleation sites on the detrital quartz grains into available pore spaces in the dolomite.

Thin section petrographic analysis and SEM review of the samples revealed carbonates containing mixtures of fossil hash, detrital quartz sand, pelloids (?), and micritic material. Dolomitization has created interparticle and intercrystalline porosity, with the pure dolomite section from 1395-1397.5' exhibiting the highest reservoir quality. Smaller detrital carbonate sand in the deeper dolomite (1401-1402.9') resulted in lower reservoir quality.

Reservoir quality varies in these samples from Poor to Good, due to variations in the detrital carbonate sand size, degree of dolomitization, and the occurrence of authigenic quartz. Natural fractures were noted in the upper limestone interval, but not in the dolomitic section.

The table below details the observed matrix reservoir quality, and the potential completion problems noted in these samples.

Potential Completion Problems

DEPTH	MATRIX RESERVOIR QUALITY	FLUID RETENTION?	INSOLUABLE RESIDUE?	SWELLING CLAY SENSITIVITY?
1387.5'	Poor	Yes, due to the low porosities of the microporous carbonate.	Yes, due to the presence of quartz in these carbonates.	Expandable clays were not present.
1387.9'				
1388.0'				
1391.6'	Fair			
1392.4'	Poor			
1393.2'				
1395.9'	Good			
1396.2'	Fair			
1397.4'	Good			
1402.6'	Poor			

Further analysis is in progress in the Acid, Geomechanics, and Special Core Analysis Laboratories, aimed at evaluating the response and effectiveness of multiple acid systems with these Big Lime cores. Results of those investigations, and associated stimulation recommendations, will be reported separately

OBJECTIVES:

Conventional wholecore segments obtained from the West Virginia Geological and Economic Survey were submitted to the Technical Services Group at the Tomball Technology Center for analysis. The objectives of this analysis were to characterize framework mineralogy, cements, clays, and porosity types present in the sample, and identify potential completion problems. Analyses conducted were stereomicroscopy, porosity and permeability measurement, acid solubility, insoluble residue analysis, thin section petrographic analysis, scanning electron microscopy/energy dispersive spectrometry (SEM/EDS), and X-ray diffraction (XRD).

Samples from this project were tested in the Geomechanics Laboratory for values of Young's Modulus and Poisson's Ratio. Additionally, samples from this project were also tested in the Acid and Special Core Analysis Laboratory (SCAL). Those results will be reported separately.

SAMPLE ANALYSIS:

Six boxes of wholecore segments were shipped to Technical Services in Tomball for evaluation. Prior to testing, the wholecore segments were photographed for documentation purposes and for coreplug location as necessary. The wholecore photographs can be viewed in Appendix Ia & Ib on pages 15-16. Following photography, 1" and 1½" diameter coreplugs were drilled from the core, while attempting to preserve the vertically slabbed surface as much as possible. The wholecore segments were then repackaged for return to the WVGES.

Routine Core Analysis Measurements

Helium porosity and gas permeability values were measured on the Big Lime coreplugs following drying. Results of the routine core analysis are included in Appendix IIa and IIb on pages 17-18. A permeability (K) versus porosity (Phi) crossplot (Figure #1, Page #5) was generated to evaluate the data. The K vs. Phi crossplot indicates that porosity and permeability in these samples has a log-normal relationship, i.e., permeability is controlled by interparticle porosity. Table #1 lists the permeability and porosity data for the samples selected for analysis. Samples selected for additional analysis are labeled on the K vs. Phi crossplot.

Table #1 - Routine Core Analysis Data for Selected 1" Plugs

DEPTH	GAS PERM millidarcies	POROSITY %	GRAIN DENSITY gm/cc
1387.50	0.02	3.6	2.72
1387.90	0.02	1.3	2.80
1388.00	0.02	1.3	2.79
1391.60	0.29	12.4	2.82
1392.40	0.02	4.2	2.79
1393.20	0.03	5.6	2.81
1395.90	0.62	13.1	2.86
1396.20	0.34	12.7	2.84
1397.40	0.70	14.8	2.84
1402.60	0.02	5.7	2.87

Figure #1 - Permeability vs. Porosity Crossplot

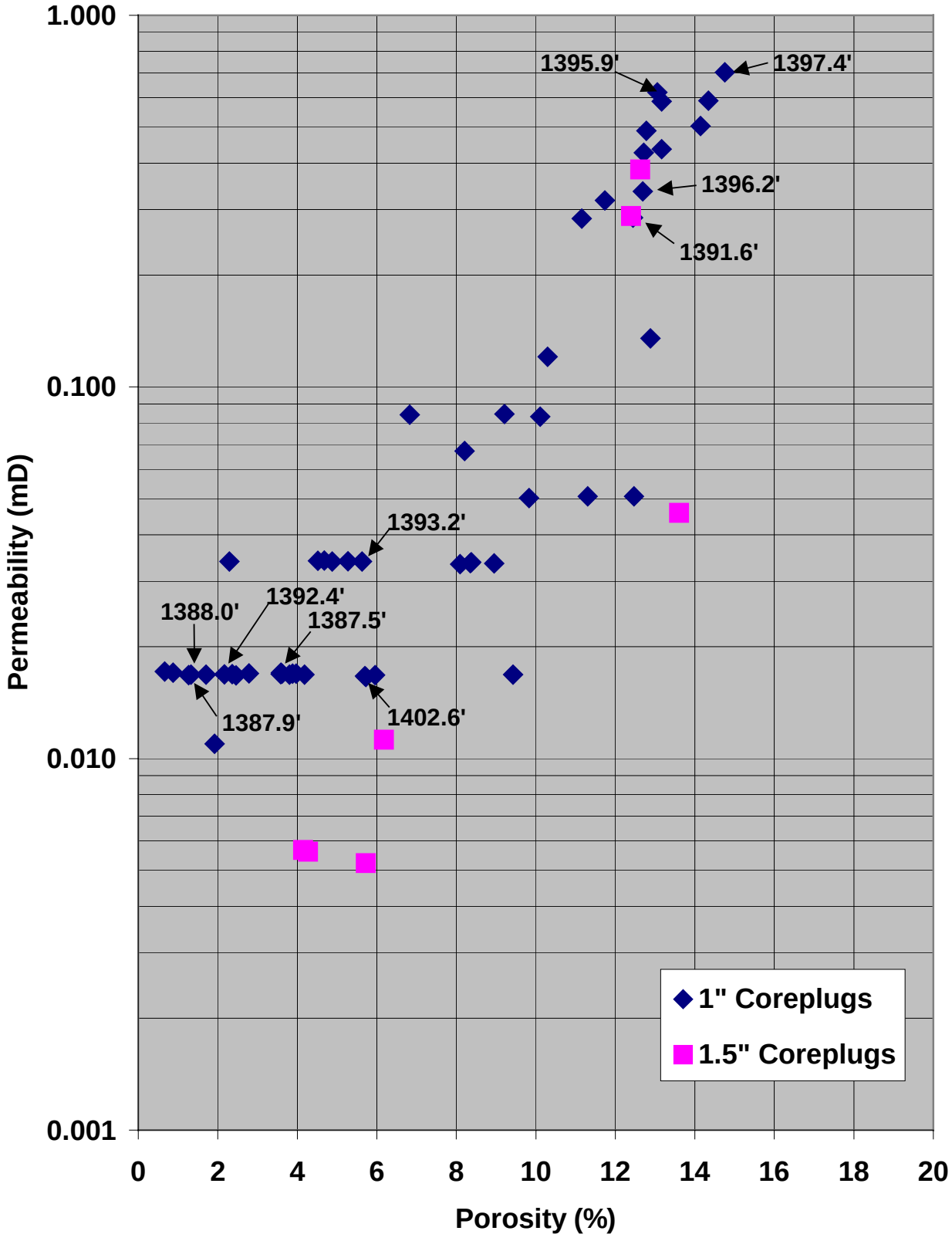

Depth plots of the core analysis data revealed trends related to both depositional environments and the diagenetic processes that the carbonates have undergone during geologic time. The graphics below are annotated to better reveal the trends.

Figure #2 - Depth versus Grain Density

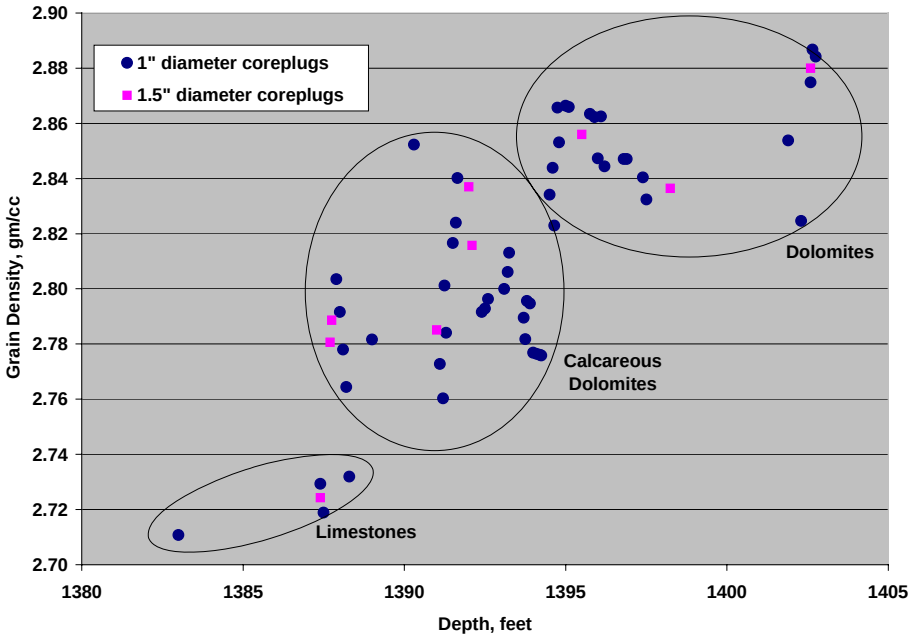

Figure #3 - Depth versus Porosity and Grain Density

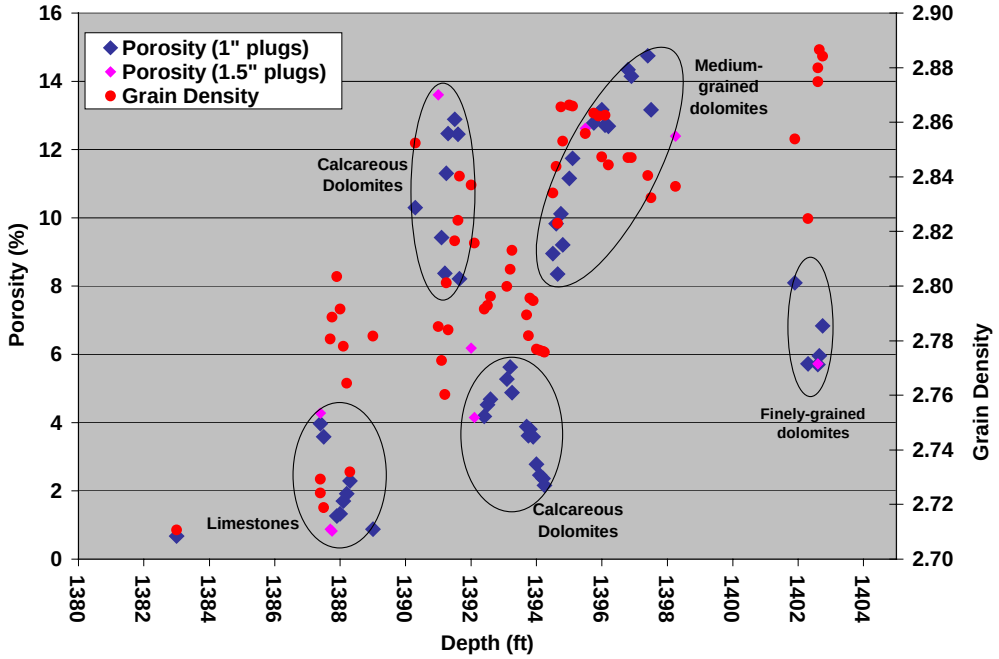

The permeability versus porosity crossplot seen in Figure #1 shows a generally distinct trend of increasing porosity equating to increasing permeability. Similar K vs. Phi crossplots any many carbonate reservoirs show a "shotgun" pattern rather than the log-normal relationship seen in Figure #1. Shotgun patterns are typically related to complex, diagenesis-related pore types such as moldic pores, microvugular pores, vugular porosity, intraparticle porosity, and solution pores. The log-normal relationship seen in these samples appears to be primarily the result of the original carbonate sand depositional environment, with some modification by the dolomitization process.

Figure #2 shows the coreplug's grain densities plotted versus depth. The mineralogical analysis presented later in this report allows the interpretations and annotations seen in the graphic. In this well, grain density increases with depth, as a function of a) dolomitization, and b) decreasing amounts of quartz grains intermixed with the carbonate sand.

Figure #3 shows both grain density and porosity plotted versus depth. This graphic indicates that porosity is controlled by several factors, including the degree of dolomitization and the size of the detrital carbonate grains.

Lithological Descriptions

Generalized lithological descriptions of the core from the six core boxes is listed below in Table #2. In-depth lithological descriptions of the Big Lime samples analyzed in this study are described in Table #3 on page #8.

Table #2 - Lithological Descriptions

Formation	Depth	Description
Big Lime	1386.0-1389.7'	Limestone; light gray, stylolitic, carbonate with medium-grained quartz lenses located in the top 0.2' of the section and a brecciated limestone band at 1387.5'
	1389.7-1391.5'	Limestone; mottled cream and light gray, stylolitic, carbonate, pyritic concretions at 1390.6'
	1391.5-1395.0'	Limestone; cream to grayish-cream, carbonate with medium-grained quartz grains, possible cross-bedding at 1394.3'
	1395.0-1398.7'	Limestone; cream colored, carbonate with few quartz grains
	1398.7-1401.0'	Missing core
	1401.0-1402.9'	Limestone; cream colored, carbonate with few quartz grains
Big Injun Sandstone	1403.5-1403.8'	Sandstone; medium-gray, pebble-conglomerate
	1403.8-1405.9'	Sandstone; red-tinted, medium to light gray, fine to medium-grained sandstone
	1405.9-1407.9'	Sandstone; reddish-gray, fine to medium-grained sandstone

Table #3 - Lithological Descriptions of Samples Selected for Analysis

Formation	Depth	Description
Big Lime	1387.5'	Limestone; microcrystalline calcite, light tanish-gray, trace amounts of quartz and Fe-rich dolomite, possibly slightly fossiliferous
	1387.9'	Limestone; microcrystalline dolomite/calcite, tanish-gray, trace amounts of quartz, dolomite is Fe-rich
	1388.0'	Limestone; microcrystalline dolomite/calcite, tanish-gray, trace amounts of quartz, dolomite is Fe-rich
	1391.6'	Limestone; microcrystalline dolomite, cream colored, minor amounts of quartz (microcrystalline and fine, rounded grains), trace amounts of calcite and plagioclase feldspar, dolomite is Fe-rich
	1392.4'	Limestone; sparry dolomite/calcite, cream colored, minor amounts of quartz (microcrystalline and fine, rounded grains), dolomite is Fe-rich
	1393.2'	Limestone; sparry dolomite/calcite, cream colored, minor amounts of quartz (microcrystalline and fine, rounded grains), dolomite is Fe-rich
	1395.9'	Dolostone; microcrystalline dolomite, cream colored, minor amounts of quartz (microcrystalline and a few fine, rounded grains), dolomite is Fe-rich
	1396.2'	Dolostone; microcrystalline dolomite, cream colored, minor amounts of quartz (microcrystalline), trace amounts of plagioclase feldspar, dolomite is Fe-rich
	1397.4'	Dolostone; microcrystalline to sparry dolomite, cream colored, minor amounts of quartz (microcrystalline), trace amounts of plagioclase feldspar, dolomite is Fe-rich
	1402.6'	Dolostone; microcrystalline dolomite, cream colored, minor amounts of quartz (microcrystalline), trace amounts of plagioclase feldspar, dolomite is Fe-rich

Mineralogical Analysis

Based upon lithology, zonation, and the routine core analysis data, ten 1" coreplug samples were selected to represent the intervals: Sub-samples were selected for mineralogical definition (XRD analysis) and rock/pore network characterization (SEM analysis and thin-section analysis). Sub-samples from the 1.5" coreplugs were also taken for acid solubility.

Acid solubility was conducted using 15% hydrochloric acid (HCl) on disaggregated material for one hour at 90°F. Data are presented in Table #4. X-ray techniques are used to determine the crystalline material content of samples. Interpreted minerals and their relative percentages are also shown in Table #4. Figure #4, is a graphical presentation of the mineralogical data from the XRD analysis.

Table #4 - Mineralogical Analysis (XRD results in weight percents), Acid Solubility Data, and Insoluble Mineralogical Analysis (XRD results in weight percents)

MINERAL PHASES	C	D	E	P	R	V	NN	QQ	TT	XX
	1387.50'	1387.90'	1388.00'	1391.60'	1392.40'	1393.20'	1395.90'	1396.20'	1397.40'	1402.60'
Quartz (SiO_2)	3	2	2	19	13	16	8	13	11	8
Plagioclase Feldspar	nd	nd	nd	1	nd	nd	tr	1	1	1
Calcite ($CaCO_3$)	94	34	35	2	32	23	nd	nd	nd	nd
Fe-Dolomite ($Ca,Fe,Mg[CO_3]_2$)	2	63	62	77	54	60	91	85	87	90
Illite	tr	tr	tr	tr	tr	tr	tr	tr	tr	tr
TOTALS	100%	100%	100%	100%	100%	100%	100%	100%	100%	100%
ACID SOLUBILITY TESTING										
SOLUBILITY	AAA	BBB	CCC	DDD	EEE	FFF	GGG	HHH	III	P
	1387.40'	1387.70'	1387.75'	1391.00'	1392.00'	1392.10'	1395.50'	1398.25'	1402.60'	1391.60'
15% HCl Solubility	96	95	94	76	90	91	86	85	93	92
INSOLUBLE MINERALS ANALYSIS										
MINERAL PHASES	#1	#2		#3	#4		#5		#6	#7
	1387.2'	1387.7'		1391.0'	1392.1'		1395.8'		1398.2'	1402.5'
Quartz (SiO_2)	62	65		56	88		80		78	51
Plagioclase Feldspar	7	4		4	2		2		2	3
Potassium Feldspar	nd	nd		1	nd		nd		nd	nd
Calcite ($CaCO_3$)	4	nd		nd	nd		nd		nd	nd
Fe-Dolomite ($Ca,Fe,Mg[CO_3]_2$)	nd	nd		7	nd		nd		nd	nd
Illite	26	30		31	9		17		19	45
TOTALS	100%	100%		100%	100%		100%		100%	100%

tr = trace, nd = not detected

Figure #4 - Mineralogical Analysis (XRD Results in Weight Percents)

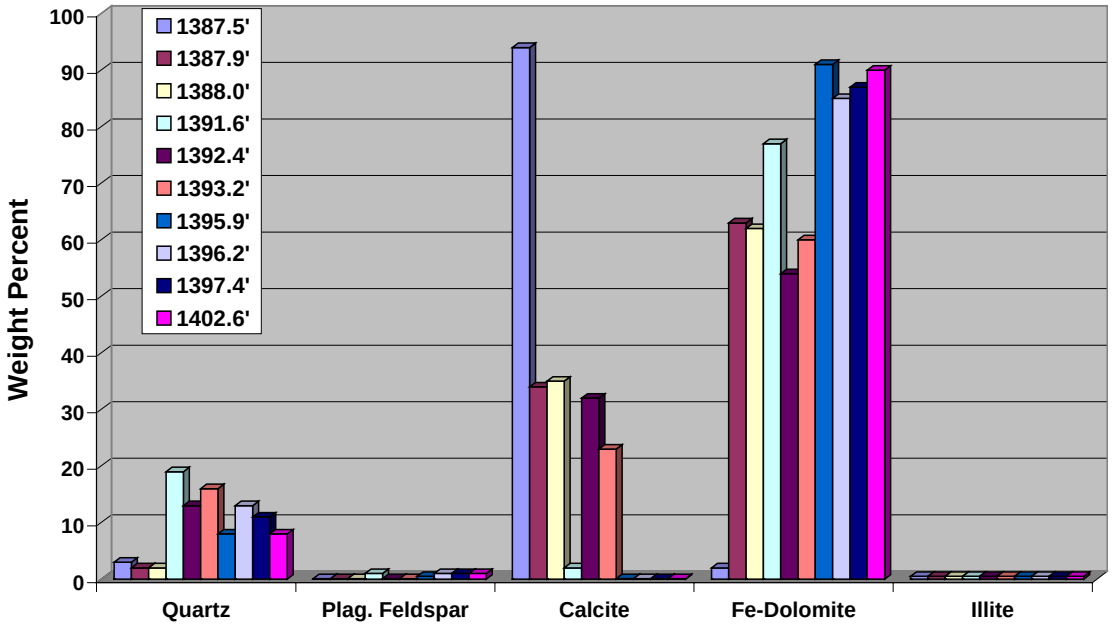

Seven samples were also selected for insoluble residue mineralogical analysis. The selected chips were digested in warm 15% HCl until the acid was spent, washed clean, and then analyzed using x-ray diffraction techniques.

Figure #5 - Mineralogical Analysis of the Insoluble Residues

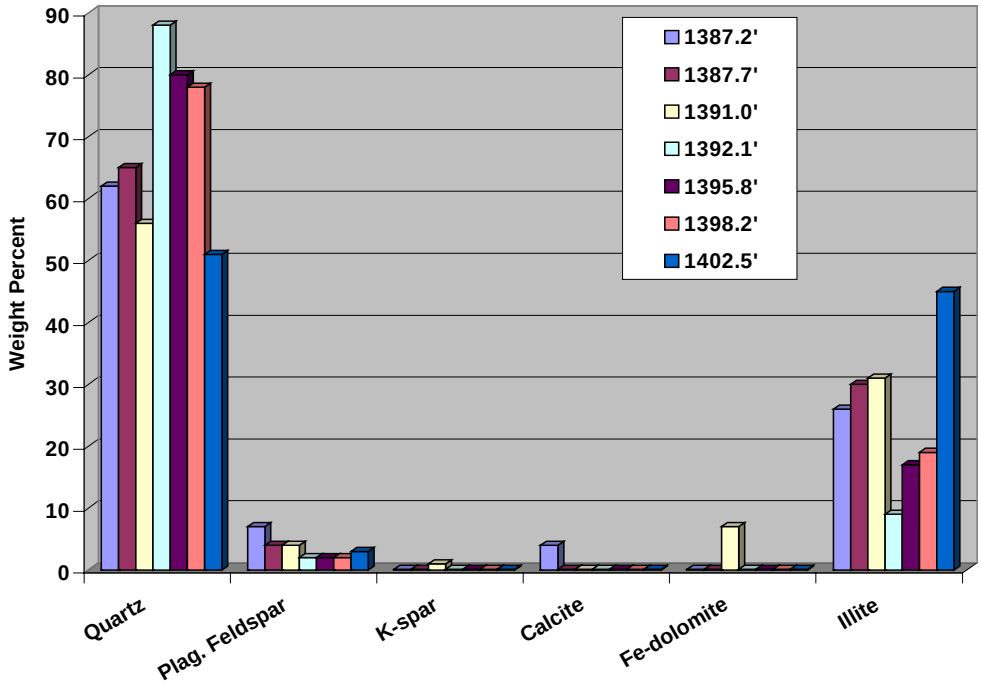

Figure #6 - SEM Review of the Insoluble Residues

(100x) **1387.2' Limestone Insolubles** **(500x)**

(30x) **1392.1' Calcareous Dolomite Insolubles** **(100x)**

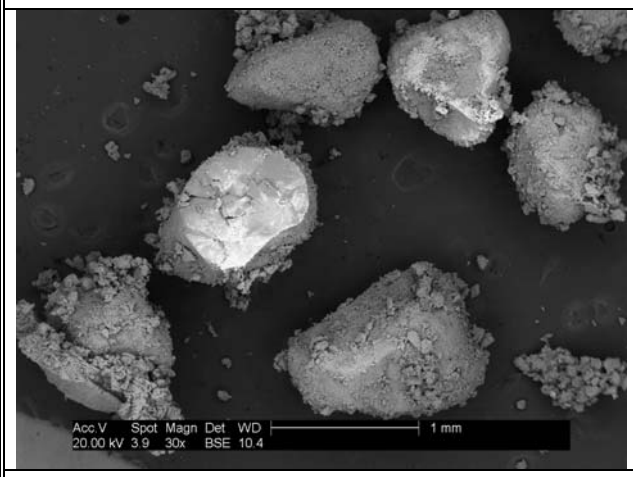

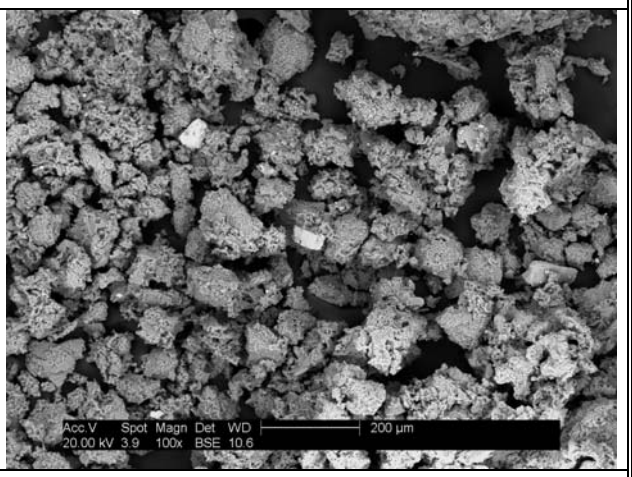

(100x) **1395.8' Dolomite Insolubles** **(100x)**

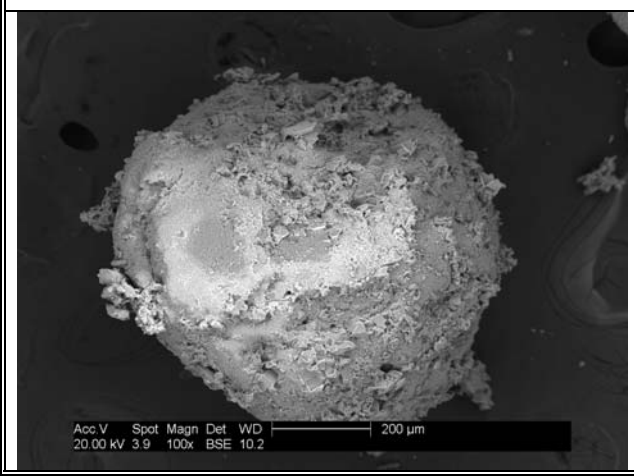

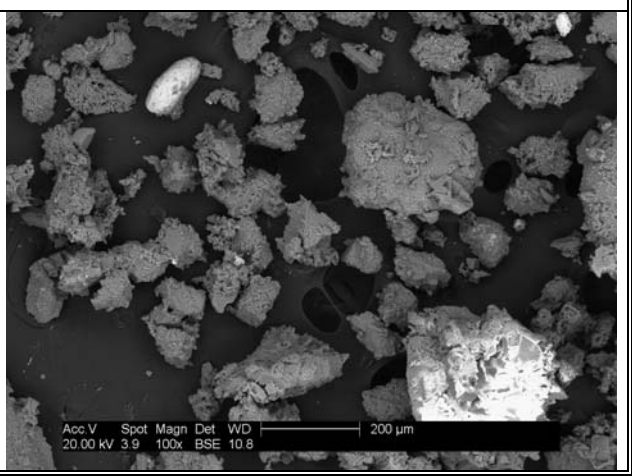

The SEM views above show the insoluble residues from three samples: 1387.2' (top of the Big Lime interval), 1392.1' (the calcareous dolomite), and 1395.8' (the porous, clean Dolomite). The original magnifications above each photograph allow comparison of the relative sizes of the

particles, and the micron bar at the bottom of each photograph enables measurement of the particle sizes. Several significant differences are visible. The insoluble material from the tight limestone at 1387.2' is composed almost exclusively of euhedral quartz crystals, which are interpreted to be authigenic crystals precipitated in the limestone from migrating silica-rich formation waters. These crystals are interpreted to be replacement deposits, where voids in the limestone were created by dissolution of pre-existing material and filled to some extent by the euhedral crystals. Note that the 500X view shows indentations in the quartz crystals where the adjoining calcite matrix prevented completion of the hexagonal quartz crystal structure.

The insoluble material in the calcareous dolomite and clean dolomite show a marked difference from the euhedral crystals present in the limestone. The two lower left-side photos show sand-sized detrital quartz grains with roughly-textured authigenic quartz crystals on their exterior surfaces. The authigenic quartz was also precipitated from silica-rich formation waters, growing from nucleation sites on the detrital quartz grains into available pore spaces in the dolomite. The botttom two 100X photographs, from the clean dolomite at 1395.8', illustrate the wide variation in the detrital quartz grain sizes.

Scanning Electron Microscopy and Thin Section Petrography

Formation chips were cleaned with hydrocarbon solvents and dried in a convection oven. Fresh surfaces were obtained by cracking the chips open; these pieces were subsequently mounted on aluminum sample holders for SEM/EDS analysis. Coreplug endtrims were saturated with blue-dyed epoxy then cut and polished for thin section analysis. The attached SEM and thin section photoplates document the rock/pore network seen in these samples, and illustrate specific examples of common features at varying magnifications. Several of the thin section slides were stained with Alizarin Red dye. Alizarin Red is used to differentiate between dolomite and calcite in limestones by staining calcite red.

Poor Interparticle Porosity

Sample 1387.5' is a fossiliferous, microcrystalline limestone consisting of calcite fossil hash, authigenic quartz crystals, and traces of anhydrite. Open interparticle pores were rare. Microporosity is the main porosity type in this limestone. A natural fracture is noted in thin-section photoplate #2. Samples 1387.9' and 1388.0' at 1.3% porosity were the lowest porosity samples analyzed. These tight calcite-rich dolomites showed no visible macroporosity and moderate microporosity. Quartz content at 2% was much lower then it is with most of the other samples. Sample 1392.4' is a fossiliferous, quartz-rich dolomite. The quartz was mainly found as distinct medium-sized quartz grains as opposed to the authigenic quartz crystals identified in other samples. Macro-pores were rare in this carbonate. Microporosity is the main porosity type. Sample 1393.2' is a fossiliferous dolomite consisting of calcite fossil hash and fine to medium grained quartz in a dolomite matrix. No visible macro-porosity was seen. The main porosity type in this dolomite was microporosity. Sample 1402.6' is a quartz-rich dolomite. The quartz in this sample is found as distinct, fine-grained quartz grains. No visible macroporosity was identified in this sample leaving microporosity as the main porosity type in this dolomite.

Fair Interparticle Porosity

Sample 1391.6' is a quartz-rich dolomite. The highest percentage of quartz (19%) was identified in this sample and was observed as distinct, sub-rounded to well rounded, coarse quartz grains

(See Photoplate 8). Constricted interparticle pore throats were more common in this sample but microporosity is still the main porosity type. Sample 1396.2' is a quartz-rich dolomite consisting of medium grained dolomite and fine to medium quartz grains. Trace amounts of illitic clay were also identified in this sample constricting open interparticle pores. The main porosity type in this dolomite is still microporosity.

Good Interparticle Porosity

Sample 1395.9' is a fine to medium grained dolomite with minor amounts of quartz. The quartz was present as distinct fine quartz grains, as well as distinct crystalline authigenic quartz. Trace amounts of fragile illitic clay were identified during the SEM analysis. The illitic clay appears to be confined to grain dissolution areas as opposed to being spread throughout the pore network. Open interparticle pores were far more common in this sample than in other samples, as can be seen in both the SEM photoplates and the thin section photoplates (pages #31-32). Microporosity adds significantly to total porosity in this sample. Sample 1397.4' is a quartz-rich, fine to medium grained dolomite. The minor amount of quartz in this sample is present as both medium-sized quartz grains and distinct crystalline authigenic quartz. The authigenic quartz and a trace amount of illitic clay have reduced primary porosity only slightly. Primary porosity in this sample is more prominent than in any other sample.

POTENTIAL COMPLETION PROBLEMS:

Listed in the table below are the potential completion problems noted in these samples. Discussion of these completion problems follows the table, **in order of importance**.

Table #5 - Potential Completion Problems

DEPTH	MATRIX RESERVOIR QUALITY	FLUID RETENTION?	INSOLUABLE RESIDUE?	SWELLING CLAY SENSITIVITY?
1387.5'	Poor	Yes, due to the low porosities of the microporous carbonate.	Yes, due to the presence of quartz in these carbonates.	Expandable clays were not present.
1387.9'				
1388.0'				
1391.6'	Fair			
1392.4'	Poor			
1393.2'				
1395.9'	Good			
1396.2'	Fair			
1397.4'	Good			
1402.6'	Poor			

- Matrix Reservoir Quality
  Samples 1387.5', 1387.9', 1388.0', 1392.4', 1393.2', and 1402.6' - The lack of dolomitization in the limestone interval (1386-87.6'), along with the porosity-reducing euhedral quartz crystals, limit the matrix porosity to Poor levels.

Samples 1391.6' and 1396.2' - The reservoir quality of these intervals is characterized as Fair due to the dolomitization of the original carbonate which has created a microporous matrix.
Samples 1395.9' and 1397.4' - The reservoir quality of these samples is characterized as Good due mainly to the increase in interparticle porosity. Small grain size and authigenic mineral precipitates still limit the total porosity in these zones.

- Natural Fractures
  Natural fractures were observed in a couple of the coreplugs drilled for this analysis, as well as in one thin section (See Photoplate 2). The natural fractures were located in the shallowest (~1387.5') portion of the Big Lime zone. Natural fractures, if present in the rest of the reservoir, will assist in draining the reservoir by connecting the matrix to artificially created hydraulic fracture pathways.

- Insoluble Residues Generated during Acidization
  Acid treatment of carbonate formations commonly results in some amount of insoluble residue, which can lower treatment effectiveness. The quartz content in these carbonates ranged from 2 to 19% and was identified as both fine to coarse grains and as distinct euhedral quartz crystals which grew in situ. Insoluble residue contents, after digestion in 15% hydrochloric acid (HCl), ranged from 51-88% quartz, 2-7% feldspar, and 9-45% illite clay.

- Water Sensitivity - Fluid Retention in Microporosity
  Because capillary forces are strong in microporosity, injected fluids may tend to be retained in these pore spaces. This has the effect of increasing water saturation (assuming that these pores are not already saturated with interstitial formation water). Increasing water saturation decreases relative permeability to hydrocarbons, thus reducing hydrocarbon deliverability.

Further analysis is in progress in the Acid, Geomechanics, and Special Core Analysis Laboratories, aimed at evaluating the response and effectiveness of multiple acid systems with these Big Lime cores. Results of those investigations, and associated stimulation recommendations, will be reported separately

---

Technology Center Report No. **06-10-0906** Reported by: BJ Davis & Laura Vestal
Requested by: Roger Myers
Location: Pittsburg, PA
Analyzed by: Dr. Gerald Braun, Amanda Seholm, Laura Vestal, David Wang, Dr. Russell Maharidge, Nathan Knudson, Jennifer Cutler, Kimberly Spurlock, BJ Davis, Vicki Johnson
Distribution: Roger Myers, Dan Kendrick, Brian Ward, Leonard Kalfayan, Bill Wood, Formation File, TTC File

Appendix Ia - Wholecore Photographs

1386-1389.5’	1389.5-1393.1	1393.1-1395.7
		

yellow bar represents 2”

Appendix Ib - Wholecore Photographs

1395.7-1398.7’	1401-1404.8’	1404.8-1407.9’
		

yellow bar represents 2”

Appendix IIa - Routine Core Analysis Data for 1" Coreplugs

DEPTH	GAS PERM millidarcies	POROSITY %	GRAIN DENSITY gm/cc
1383.00	0.02	0.7	2.71
1387.40	0.02	4.0	2.73
1387.50	0.02	3.6	2.72
1387.90	0.02	1.3	2.80
1388.00	0.02	1.3	2.79
1388.10	0.02	1.7	2.78
1388.20	0.01	1.9	2.76
1388.30	0.03	2.3	2.73
1389.00	0.02	0.9	2.78
1390.30	0.12	10.3	2.85
1391.10	0.02	9.4	2.77
1391.20	0.03	8.4	2.76
1391.25	0.05	11.3	2.80
1391.30	0.05	12.5	2.78
1391.50	0.14	12.9	2.82
1391.60	0.29	12.4	2.82
1391.65	0.07	8.2	2.84
1392.40	0.02	4.2	2.79
1392.50	0.03	4.5	2.79
1392.60	0.03	4.7	2.80
1393.10	0.03	5.3	2.80
1393.20	0.03	5.6	2.81
1393.25	0.03	4.9	2.81
1393.70	0.02	3.9	2.79
1393.75	0.02	3.6	2.78
1393.80	0.02	3.8	2.80
1393.90	0.02	3.6	2.79
1394.00	0.02	2.8	2.78
1394.10	0.02	2.5	2.78
1394.20	0.02	2.4	2.78
1394.25	0.02	2.2	2.78
1394.50	0.03	9.0	2.83
1394.60	0.05	9.8	2.84
1394.65	0.03	8.4	2.82
1394.75	0.08	10.1	2.87
1394.80	0.08	9.2	2.85
1395.00	0.28	11.2	2.87
1395.10	0.32	11.7	2.87
1395.75	0.49	12.8	2.86
1395.90	0.62	13.1	2.86
1396.00	0.59	13.2	2.85
1396.10	0.43	12.7	2.86

Appendix IIa - Routine Core Analysis Data for 1" Coreplugs (Continued)

DEPTH	GAS PERM millidarcies	POROSITY %	GRAIN DENSITY gm/cc
1396.20	0.34	12.7	2.84
1396.80	0.59	14.3	2.85
1396.90	0.50	14.1	2.85
1397.40	0.70	14.8	2.84
1397.50	0.44	13.2	2.83
1401.90	0.03	8.1	2.85
1402.30	0.02	5.7	2.82
1402.60	0.02	5.7	2.87
1402.65	0.02	6.0	2.89
1402.75	0.08	6.8	2.88

Appendix IIb - Routine Core Analysis Data for 1.5" Plugs

DEPTH	GAS PERM millidarcies	POROSITY %	GRAIN DENSITY gm/cc
1387.40	0.01	4.3	2.72
1387.70	*	0.9	2.78
1387.75	*	0.8	2.79
1391.00	0.05	13.6	2.79
1392.00	0.01	6.2	2.84
1392.10	0.01	4.1	2.82
1395.50	0.38	12.6	2.86
1398.25	0.29	12.4	2.84
1402.60	0.01	5.7	2.88

* Plugs were irregular and were not suitable for permeability measurement.

PHOTOPLATE 1 - SCANNING ELECTRON MICROSCOPE PHOTOMICROGRAPHS

Big Lime Formation - 1387.50 ft. - (3.6%, 0.02mD)

VIEW A : Very few open interparticle pores were identified in this microcrystalline limestone. Authigenic quartz crystals (peaked crystals) have further reduced interparticle porosity. Large calcite crystals (center) were also identified within the microcrystalline matrix.

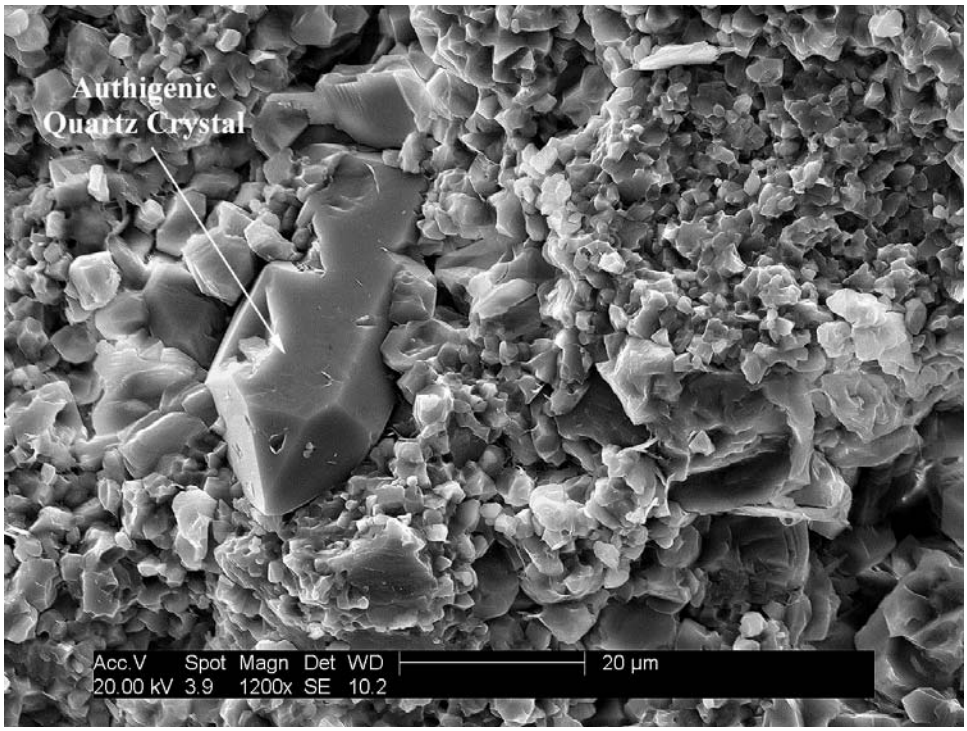

VIEW B : Microporosity is the main porosity type in this limestone.

PHOTOPLATE 2 - THIN SECTION ANALYSIS PHOTOMICROGRAPHS

Big Lime Formation - 1387.50 ft. - (3.6%, 0.02mD)

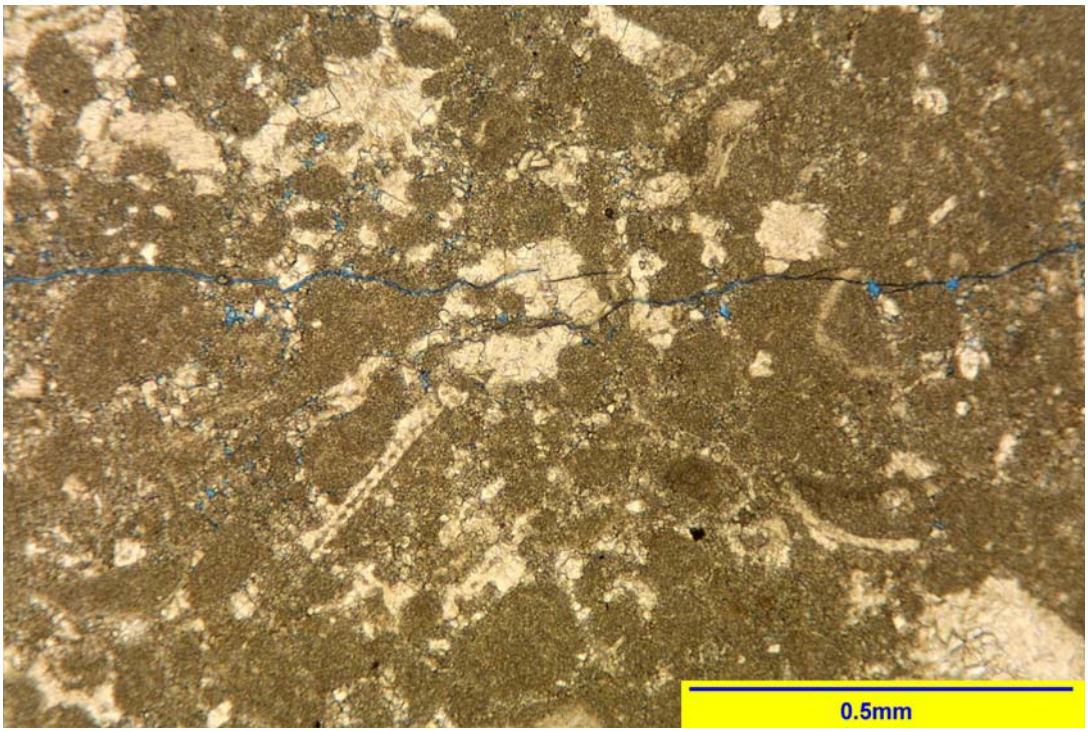

VIEW A : 90x - General view of a fine grained fossil-rich limestone consisting of calcite fossil hash and traces of anhydrite in a fine grained calcite matrix. Note fracture.

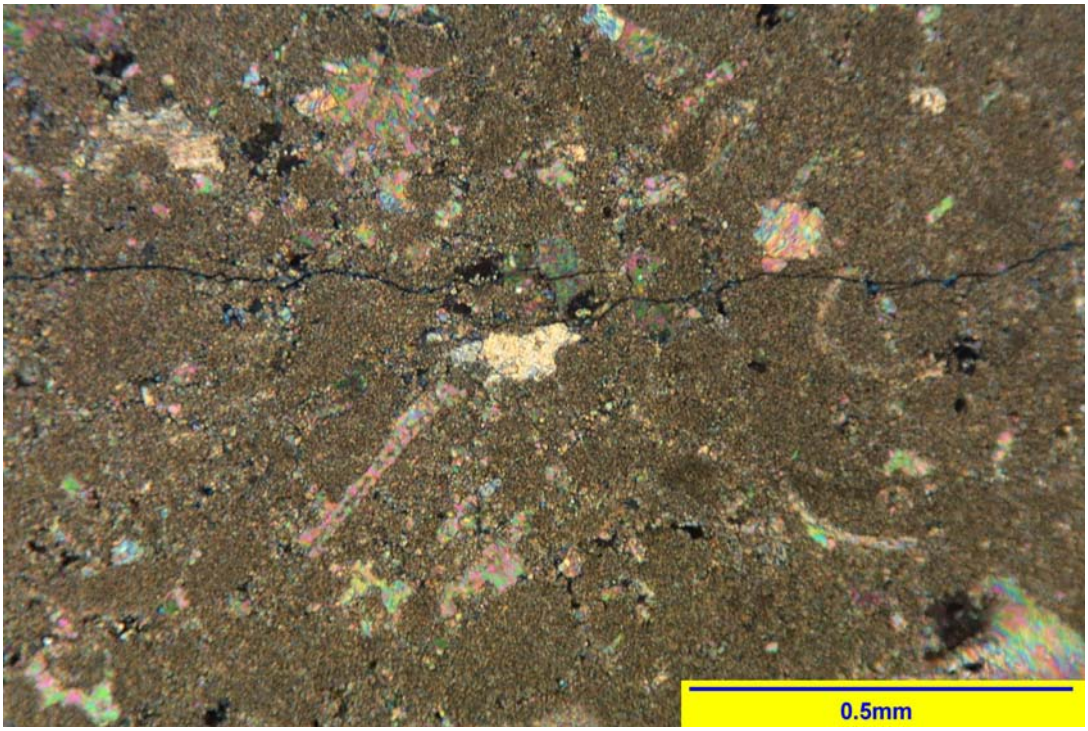

VIEW B : 90x - Cross-polarized view of above. Low-relief grain at center is anhydrite.

PHOTOPLATE 3 - SCANNING ELECTRON MICROSCOPE PHOTOMICROGRAPHS

Big Lime Formation - 1387.90 ft. - (1.3%, 0.02mD)

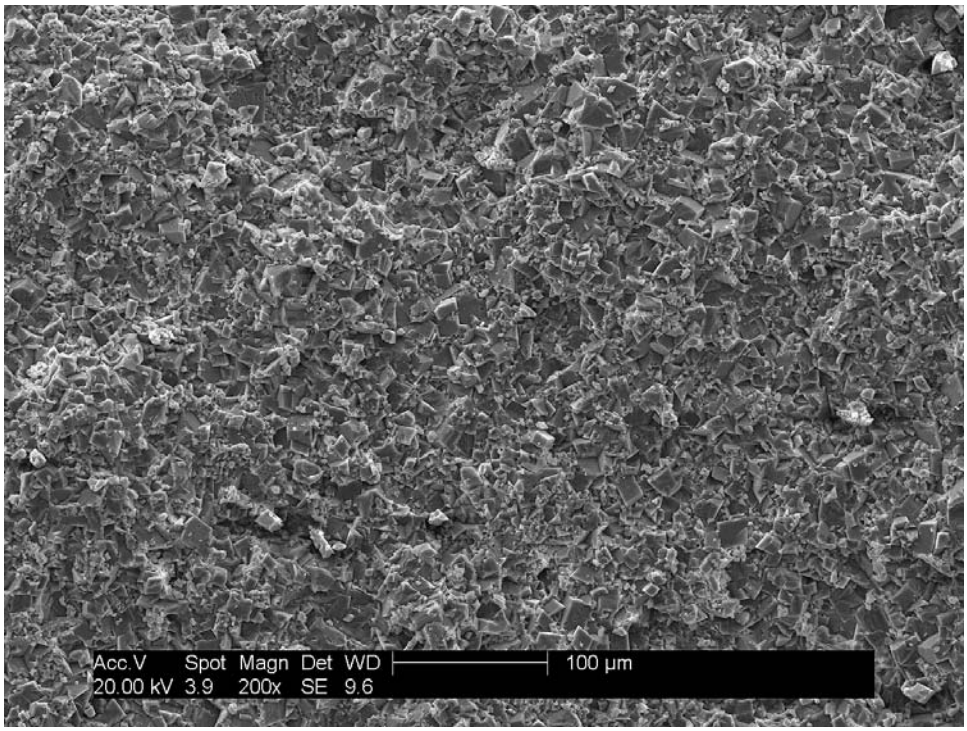

VIEW A : Interparticle porosity is considered Poor in this Fe-dolomite-rich limestone. Microporosity is the main porosity type in this zone.

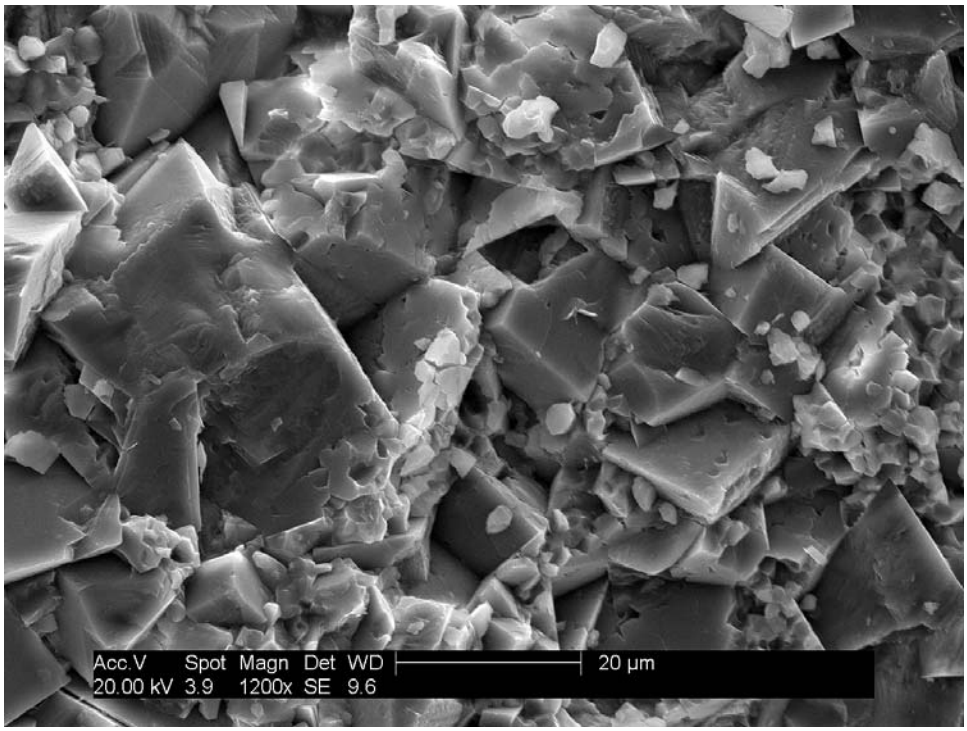

VIEW B : In this close-up view the large rhombohedral crystals are the Fe-rich dolomite crystals while the calcite has been identified in the form of small micro-crystals. Microporosity can be seen between these small micro-crystals.

PHOTOPLATE 4 - THIN SECTION ANALYSIS PHOTOMICROGRAPHS

Big Lime Formation - 1387.90 ft. - (1.3%, 0.02mD)

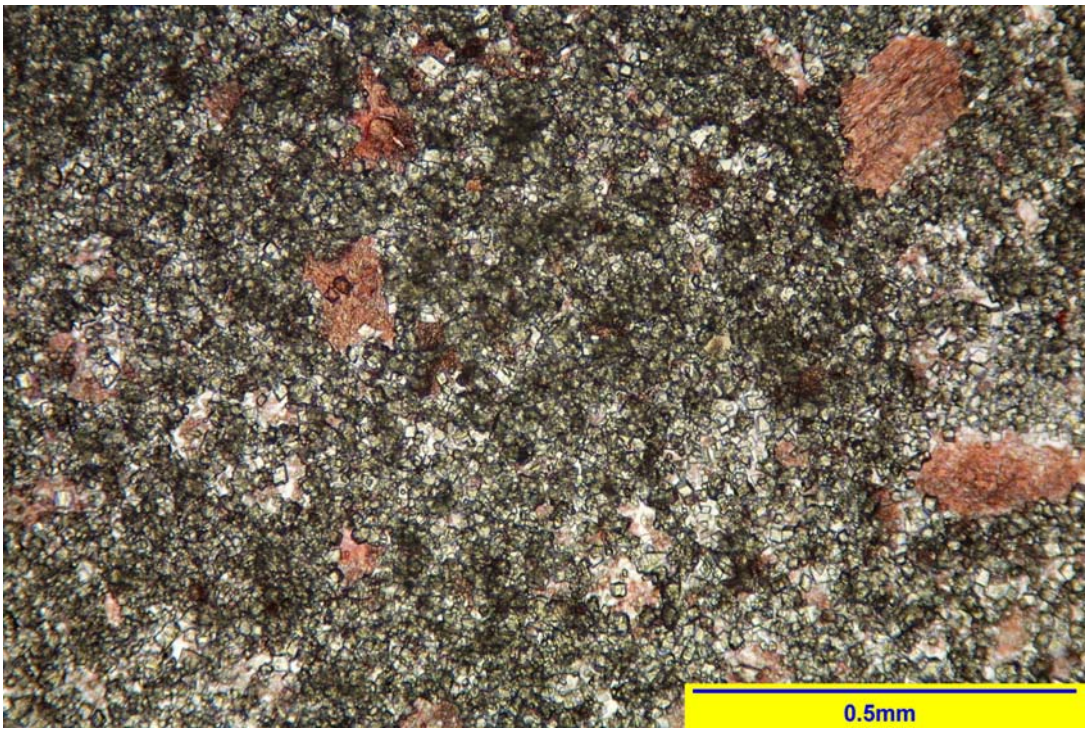

VIEW A : 90x - General view showing a calcite -rich fine grained dolomite consisting of medium, grained calcite (possibly fossil hash, stained with Alizarin Red) in a fine grained dolomite matrix.

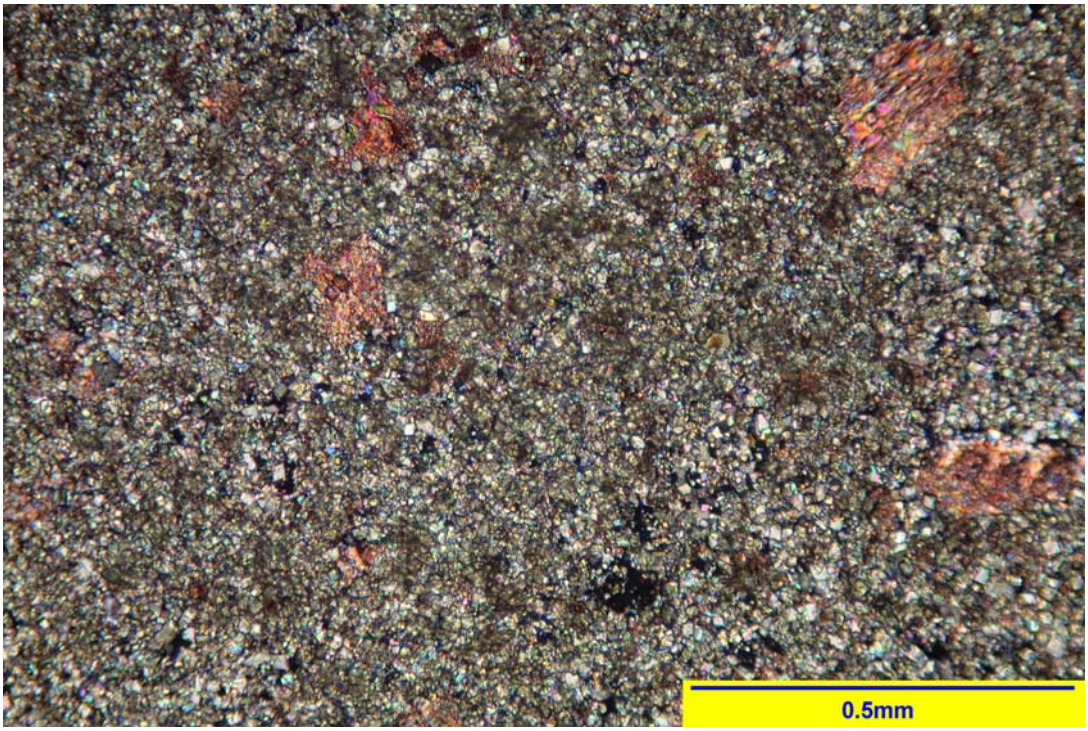

VIEW B : 90x - Cross-polarized view of above. Note: No visible porosity. Under cross-polarized light dolomite and calcite crystals display high birefringence colors (pinks, greens, blues, etc.), due to this mineral characteristic the blue in this photomicrograph is carbonate birefringence and not porosity.

PHOTOPLATE 5 - SCANNING ELECTRON MICROSCOPE PHOTOMICROGRAPHS

Big Lime Formation - 1388.00 ft. - (1.3%, 0.02mD)

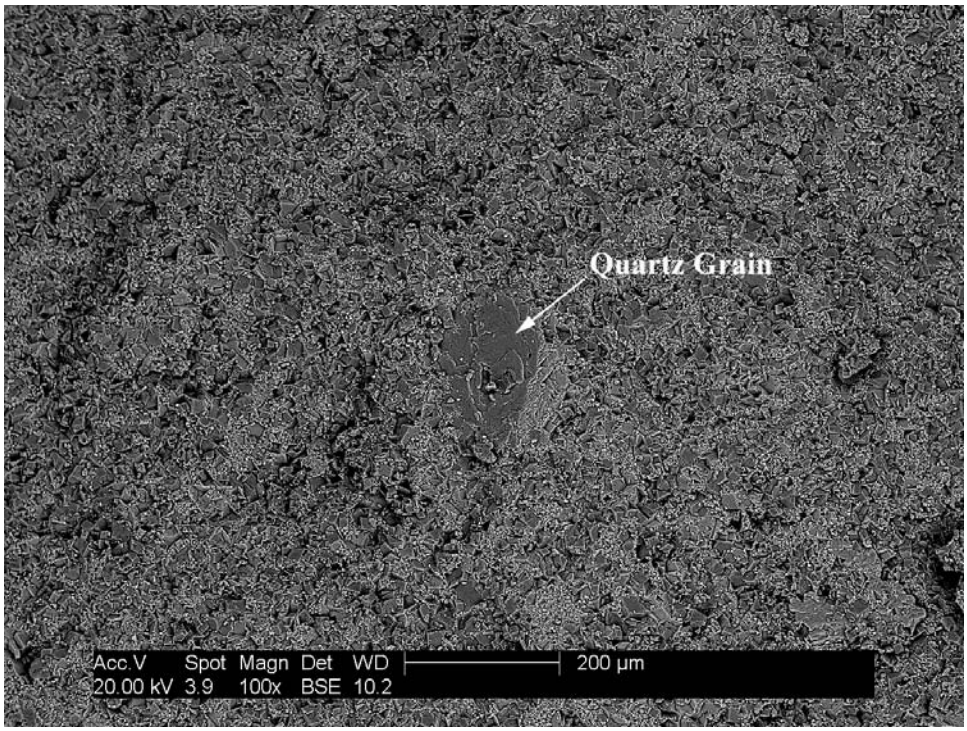

VIEW A : Interparticle porosity in this Fe-dolomite-rich limestone is Poor. The light colored, microcrystalline "grains" represent calcite, while the darker gray, rhombohedral crystals represent the Fe-dolomite. Large quartz grains, as seen in the center of this photomicrograph, become more dominant in the lower zones.

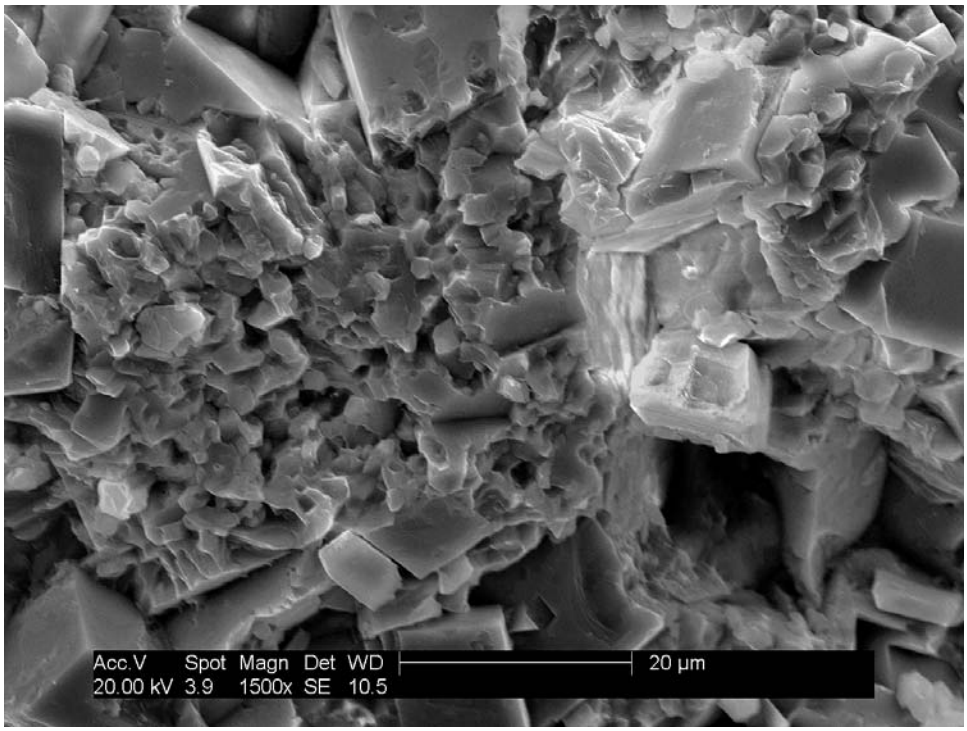

VIEW B : A microporous calcite is surrounded by rhombohedral Fe-rich dolomite crystals in this close-up view.

PHOTOPLATE 6 - THIN SECTION ANALYSIS PHOTOMICROGRAPHS

Big Lime Formation - 1388.00 ft. - (1.3%, 0.02mD)

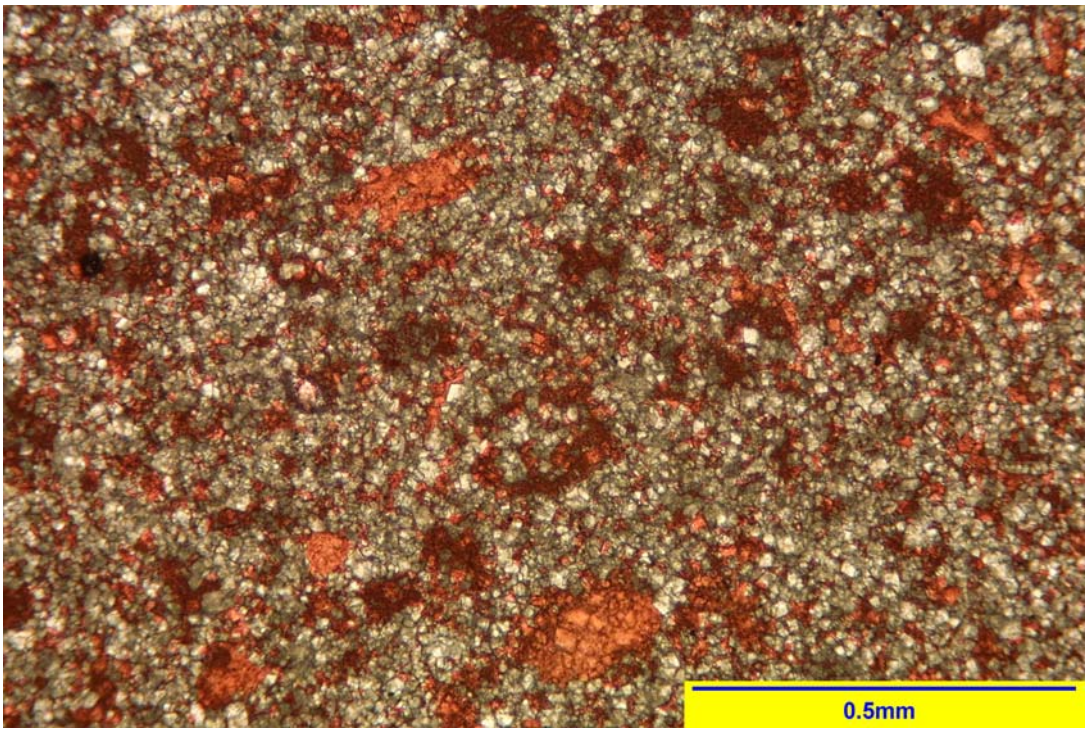

VIEW A : 90x - General view, stained with Alizarin Red, showing a very fine calcite-rich dolomite consisting calcite fossil hash in a very fine grained dolomite matrix.

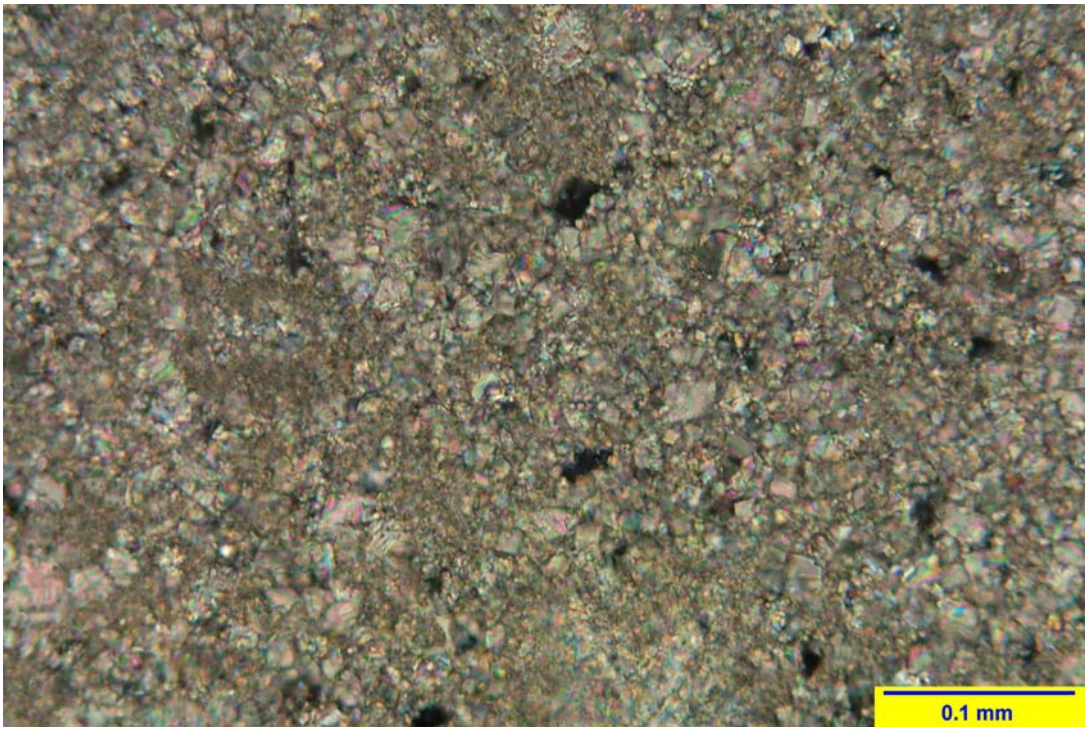

VIEW B : 240x - Cross-polarized, close-up view prior to being stained with Alizarin Red dye. Note: No macro-porosity.

PHOTOPLATE 7 - SCANNING ELECTRON MICROSCOPE PHOTOMICROGRAPHS

Big Lime Formation - 1391.60 ft. - (12.4%, 0.29mD)

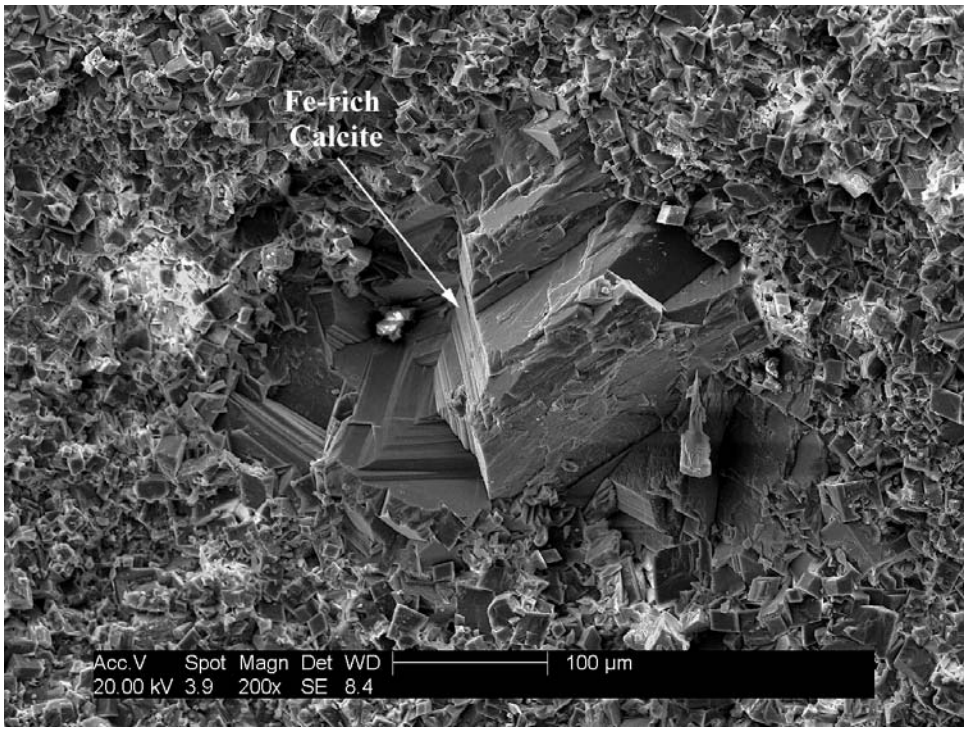

VIEW A : Interparticle porosity in this Fe-dolomite is considered Fair. The calcite in this zone consists of large iron-rich crystals instead of the micro-crystals identified in previous zones.

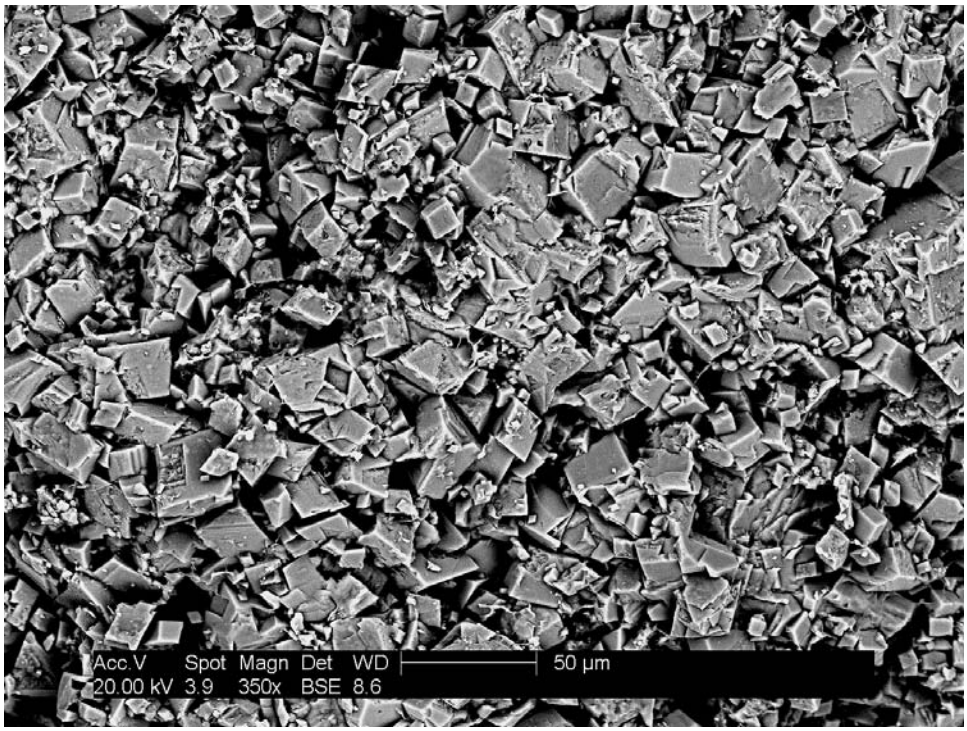

VIEW B : The main mineralogical component of this zone is Fe-rich dolomite. Quartz (19% of total) has also been identified in this sample and is found as distinct coarse quartz grains (as seen in thin section on the following page).

PHOTOPLATE 8 - THIN SECTION ANALYSIS PHOTOMICROGRAPHS

Big Lime Formation - 1391.60 ft. - (12.4%, 0.29mD)

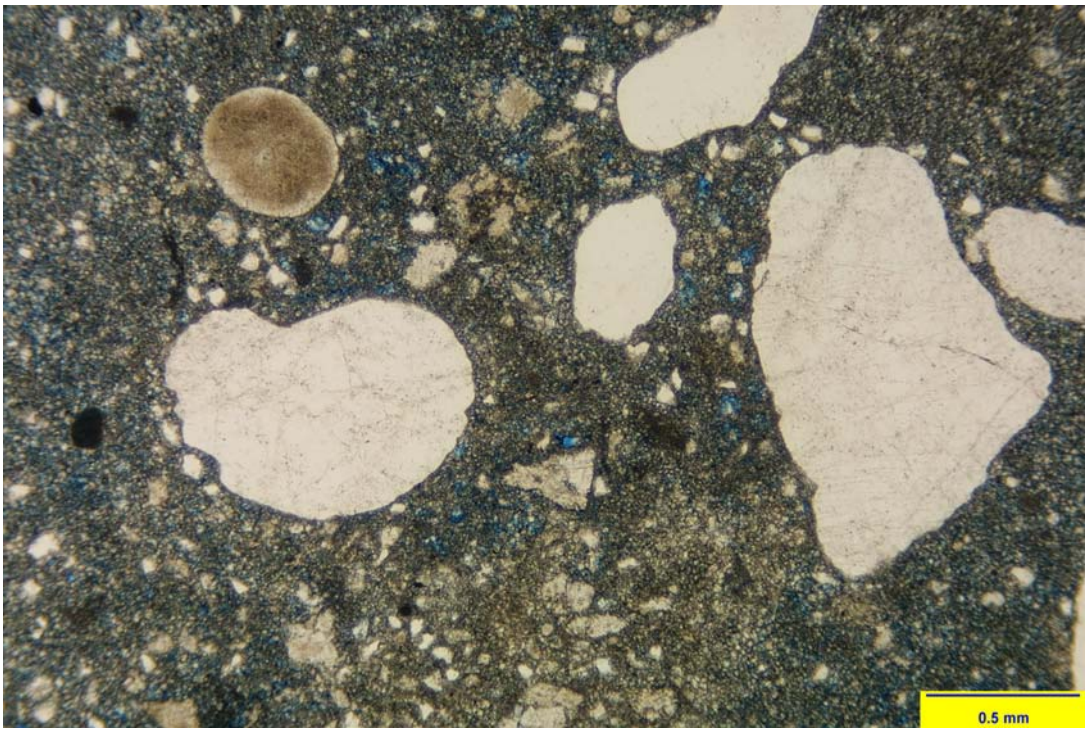

VIEW A : 40x - General view showing a slightly porous fine to medium grained quartzose dolomite consisting of subrounded to rounded, coarse grained, quartz in a fine grained dolomite matrix.

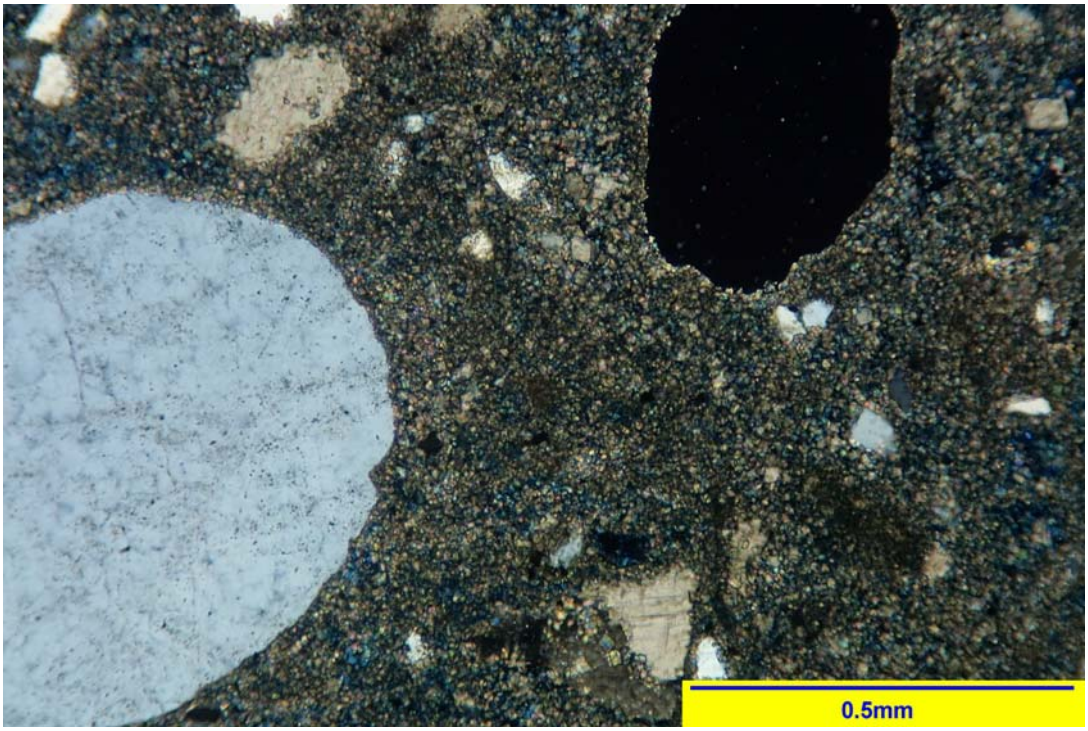

VIEW B : 90x - Cross-polarized, close-up from the center of View A.

PHOTOPLATE 9 - SCANNING ELECTRON MICROSCOPE PHOTOMICROGRAPHS

Big Lime Formation - 1392.40 ft. - (4.2%, 0.02mD)

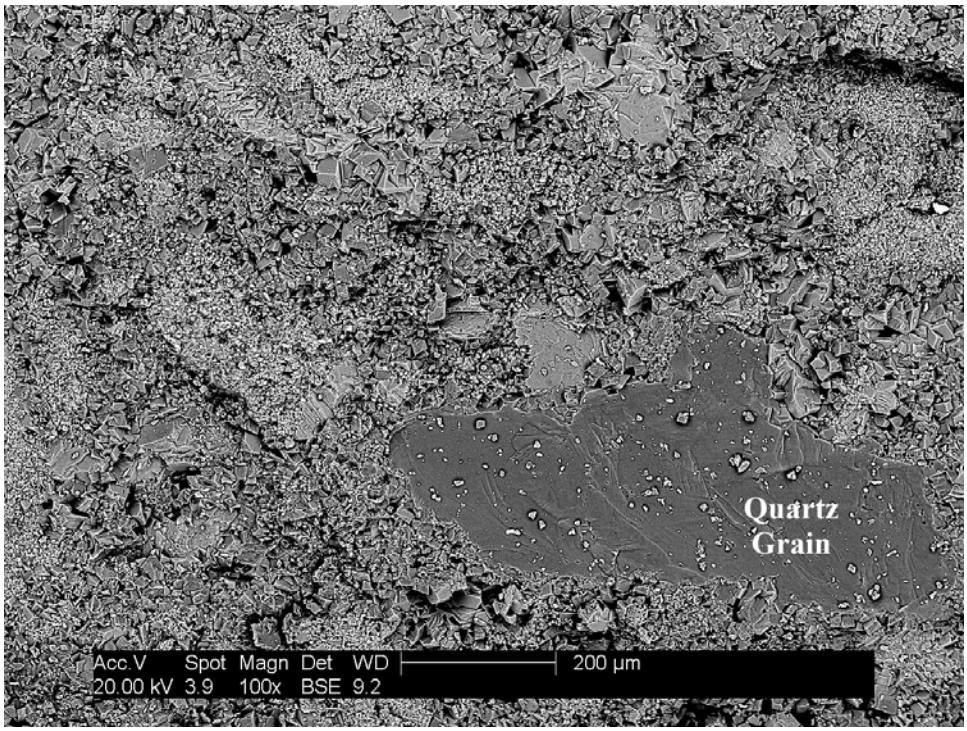

VIEW A : A quartz grain can be seen here surrounded by a mixture of microcrystalline calcite (white) and rhombohedral Fe-dolomite crystals (light to medium gray). Interparticle porosity is considered Poor in this zone at 4.2%.

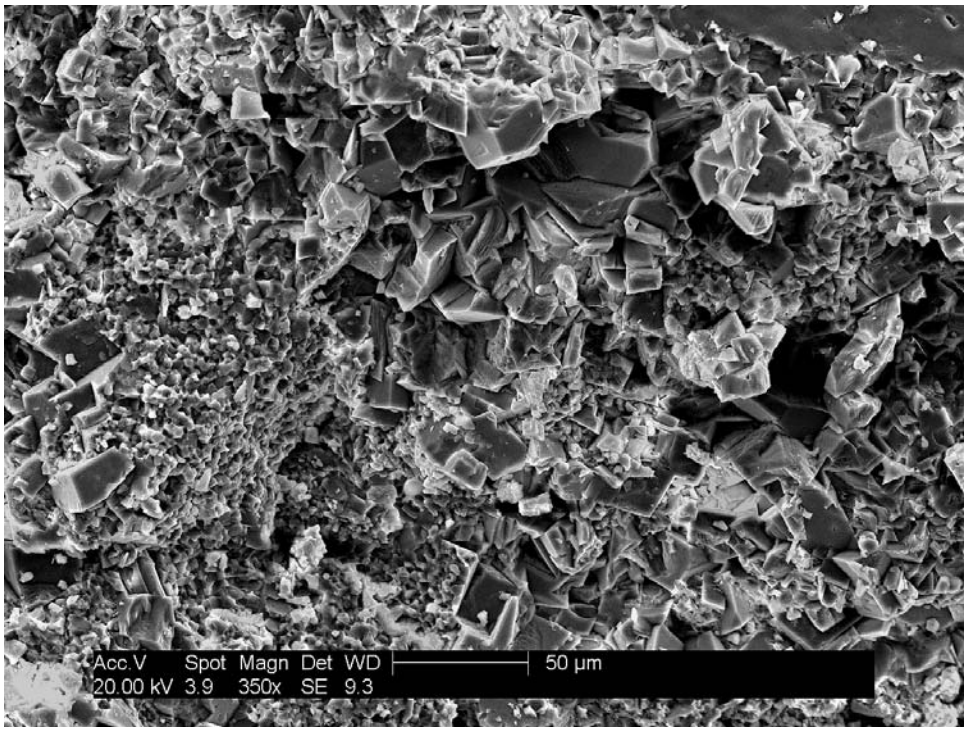

VIEW B : The main porosity is microporosity as seen here in this close-up image from the bottom-center of View A.

PHOTOPLATE 10 - THIN SECTION ANALYSIS PHOTOMICROGRAPHS

Big Lime Formation - 1392.40 ft. - (4.2%, 0.02mD)

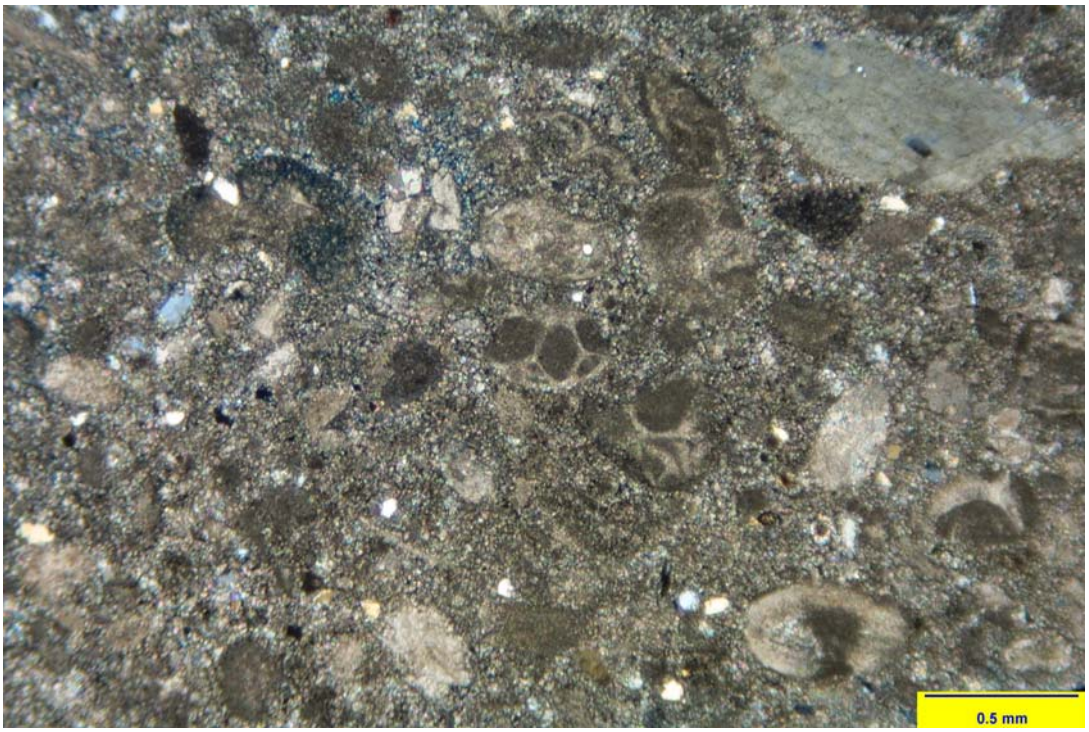

VIEW A : 40x - Cross-polarized, general view showing a fine to medium grained quartzose dolomite consisting of medium grained quartz (generally monocrystalline) and fossil "hash" in a fine grained carbonate matrix. Note the chambered fossil in center of image.

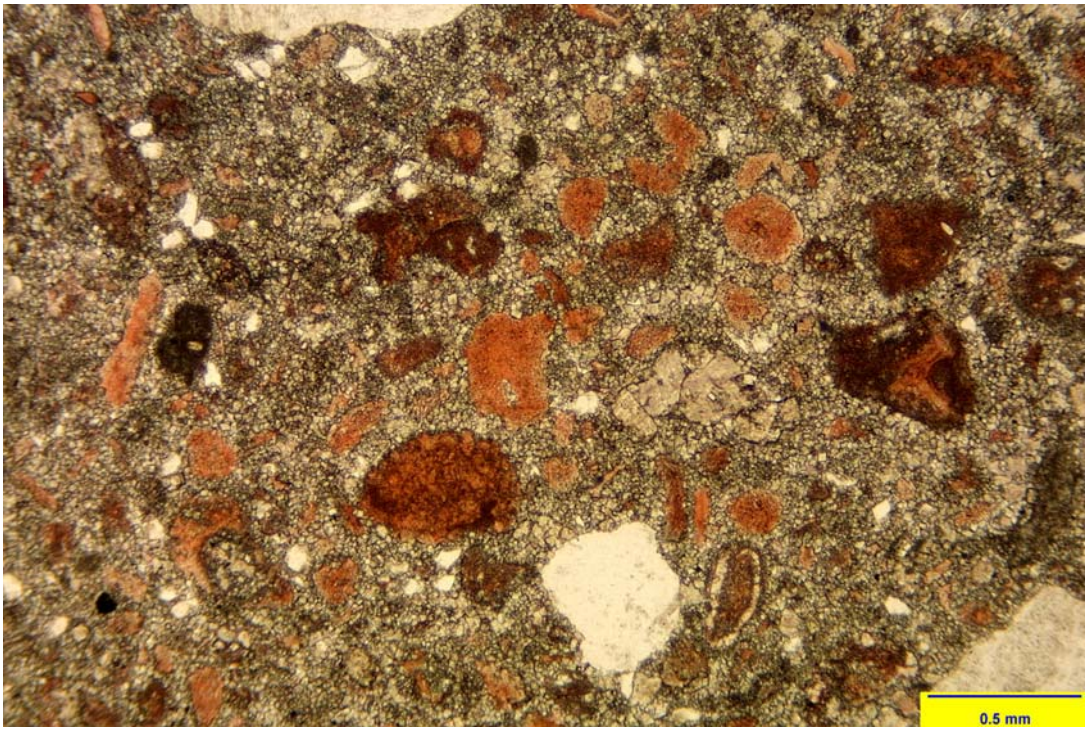

VIEW B : 40x - The calcite fossil "hash" is stained red with Alizarin Red dye.

PHOTOPLATE 11 - SCANNING ELECTRON MICROSCOPE PHOTOMICROGRAPHS

Big Lime Formation - 1393.20 ft. - (5.6%, 0.03mD)

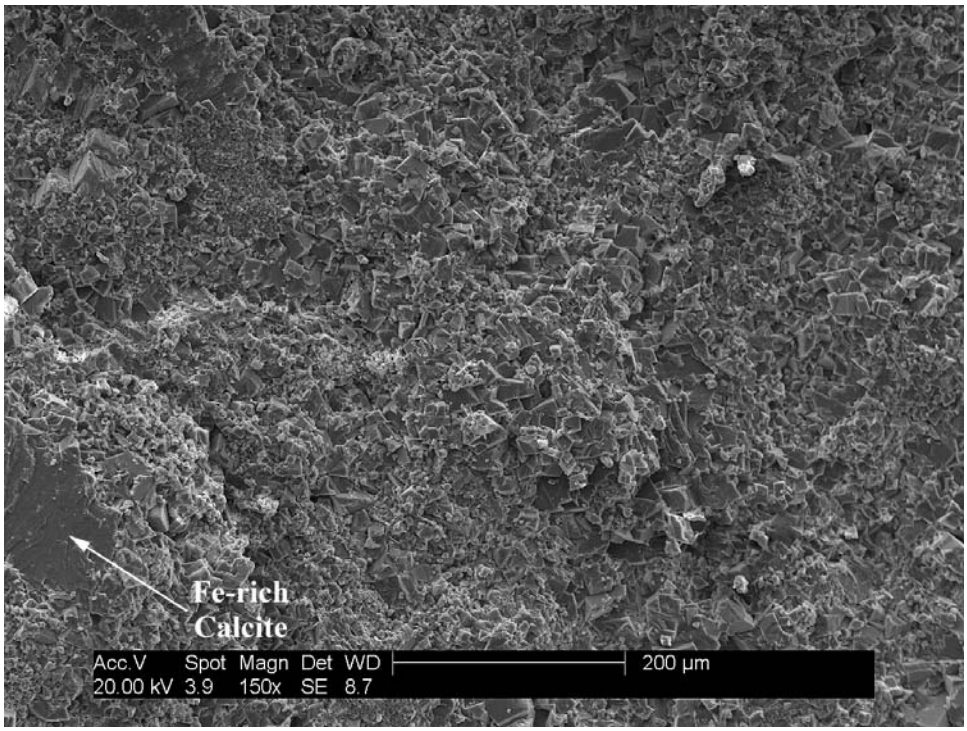

VIEW A : Interparticle porosity is considered Poor in this Fe-dolomite-rich limestone. "Grain size" in this zone varies from large Fe-rich calcite crystals to microcrystalline calcite. The rhombohedral, Fe-rich, dolomite crystals comprise about 60% of the total mineralogy in this zone.

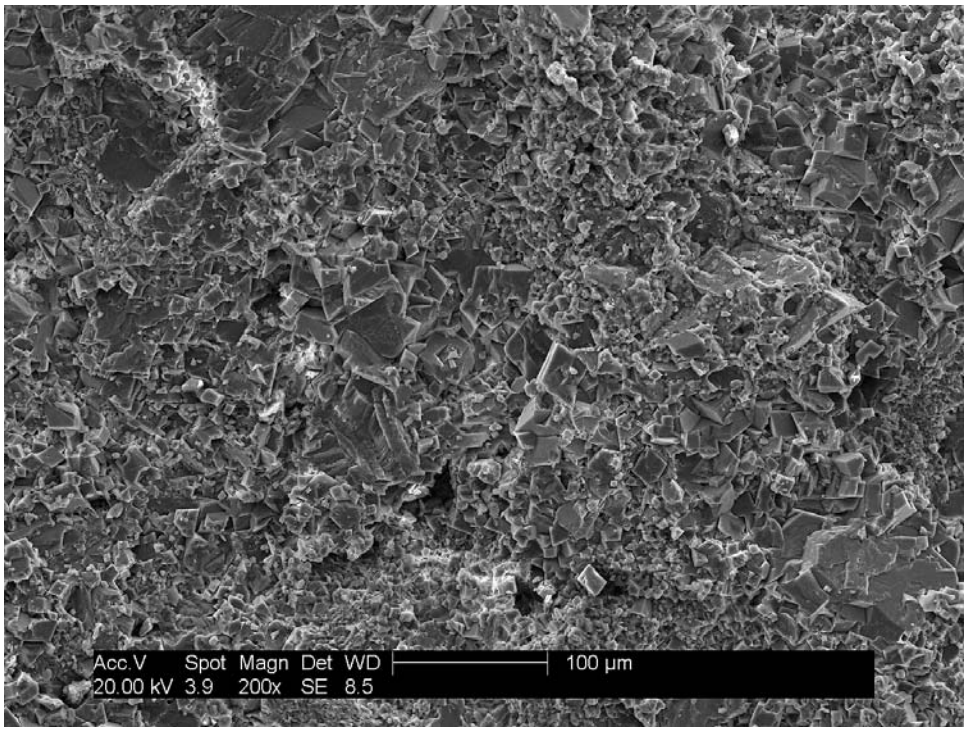

VIEW B : Several areas of open, interparticle pore space can be seen in this view, however a significant portion of the porosity consists of microporosity.

PHOTOPLATE 12 - THIN SECTION ANALYSIS PHOTOMICROGRAPHS

Big Lime Formation - 1393.20 ft. - (5.6%, 0.03mD)

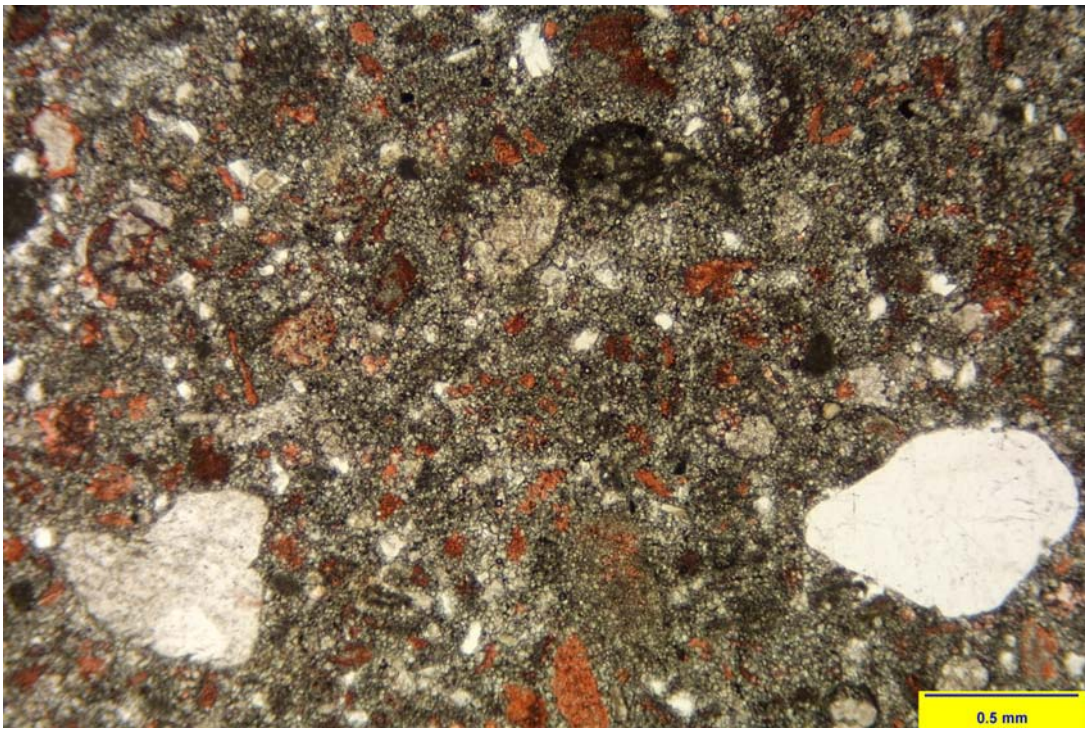

VIEW A : 40x - General view, with alizarin red stain, showing a fossiliferous dolomite consisting of calcite fossil "hash" with fine to coarse grained quartz.

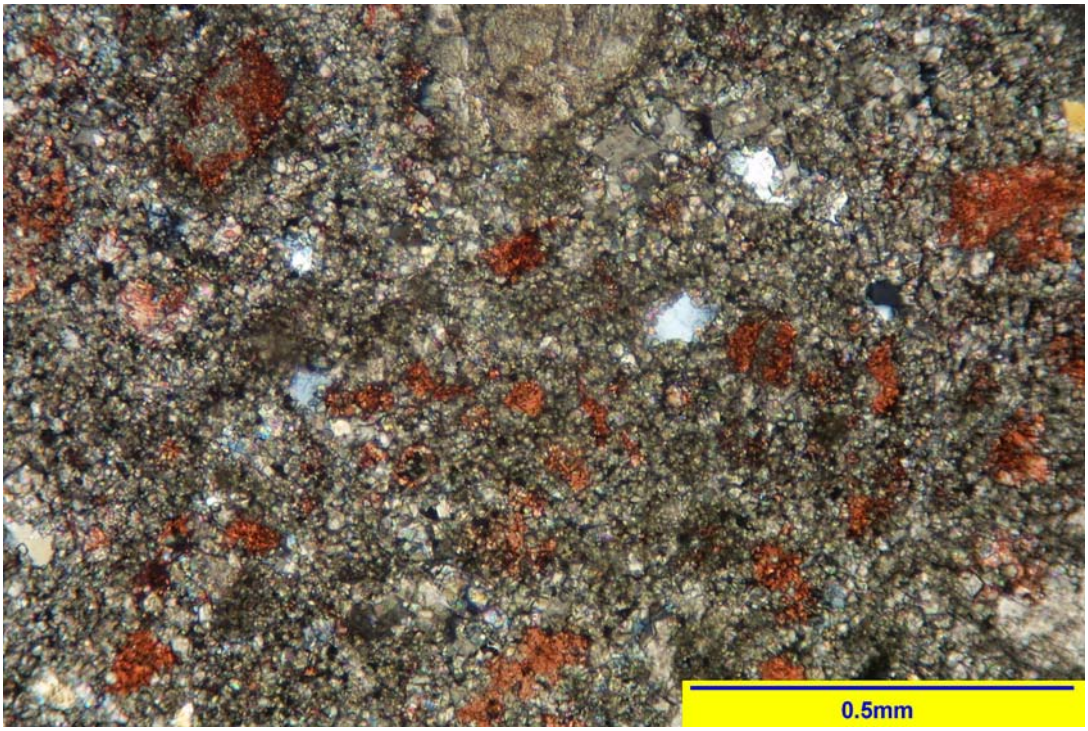

VIEW B : 90x- Close-up view from center above. Note: No visible macro-porosity.

PHOTOPLATE 13 - SCANNING ELECTRON MICROSCOPE PHOTOMICROGRAPHS

Big Lime Formation - 1395.90 ft. - (13.1%, 0.62mD)

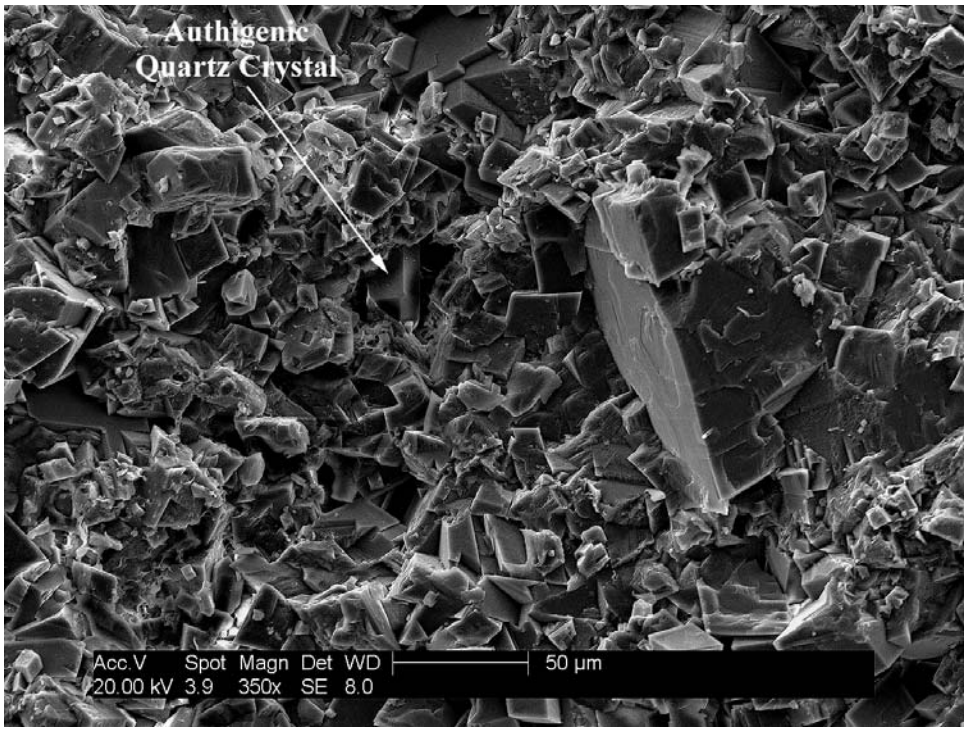

VIEW A : Interparticle porosity is considered Good in this Fe-rich dolomite. Quartz and dolomite were the main components of this zone. Quartz was identified in the form of quartz overgrowth crystals.

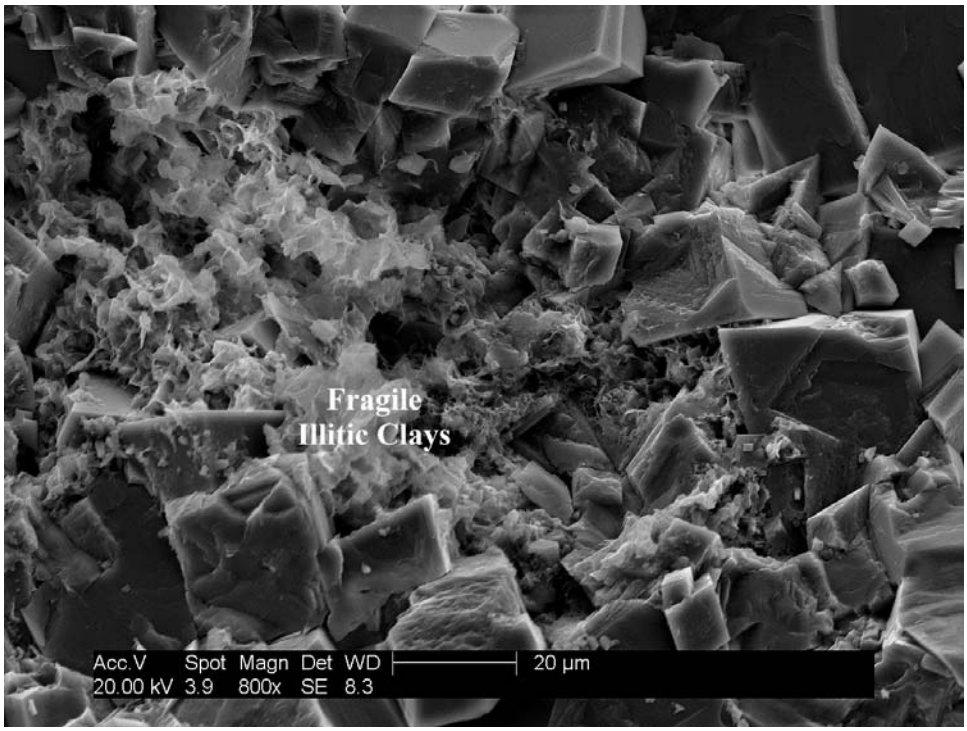

VIEW B : Fragile illitic clay was identified filling open pore space and creating microporosity in this dolomite, however clay content was found only in trace amounts during x-ray diffraction analysis, indicating that the clays are an insignificant component of this rock.

PHOTOPLATE 14 - THIN SECTION ANALYSIS PHOTOMICROGRAPHS

Big Lime Formation - 1395.90 ft. - (13.1%, 0.62mD)

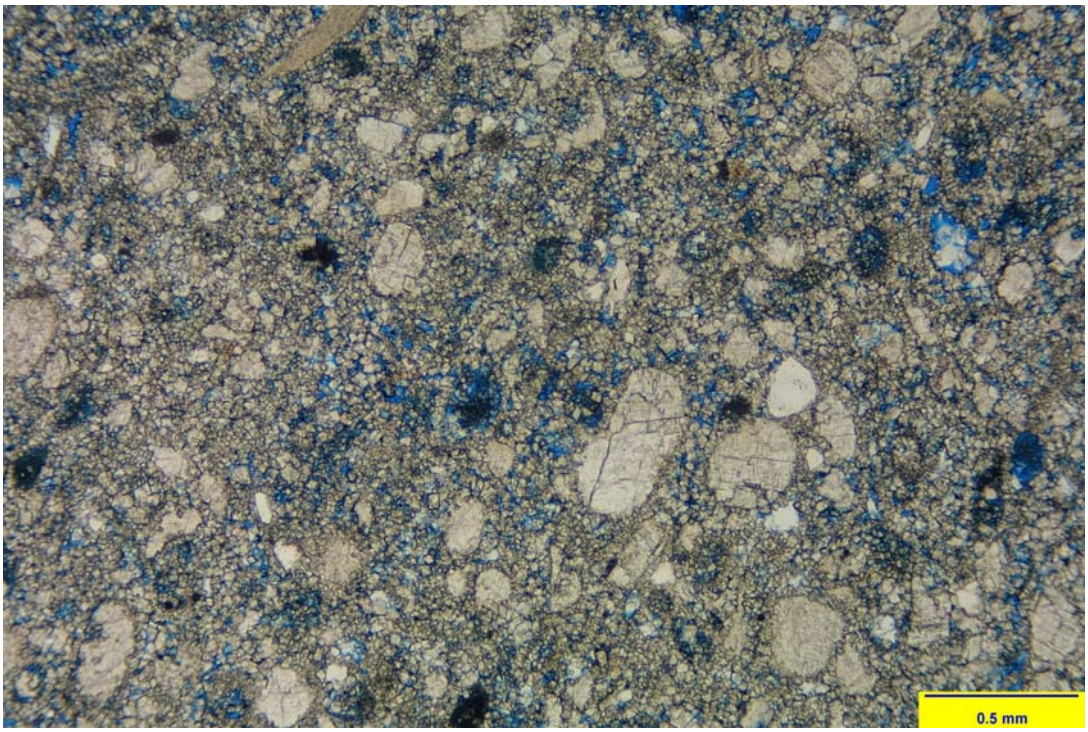

VIEW A : 40x - General view showing a porous, fine to medium grained dolomite containing a minor to trace amount of fine to medium grained monocrystalline quartz.

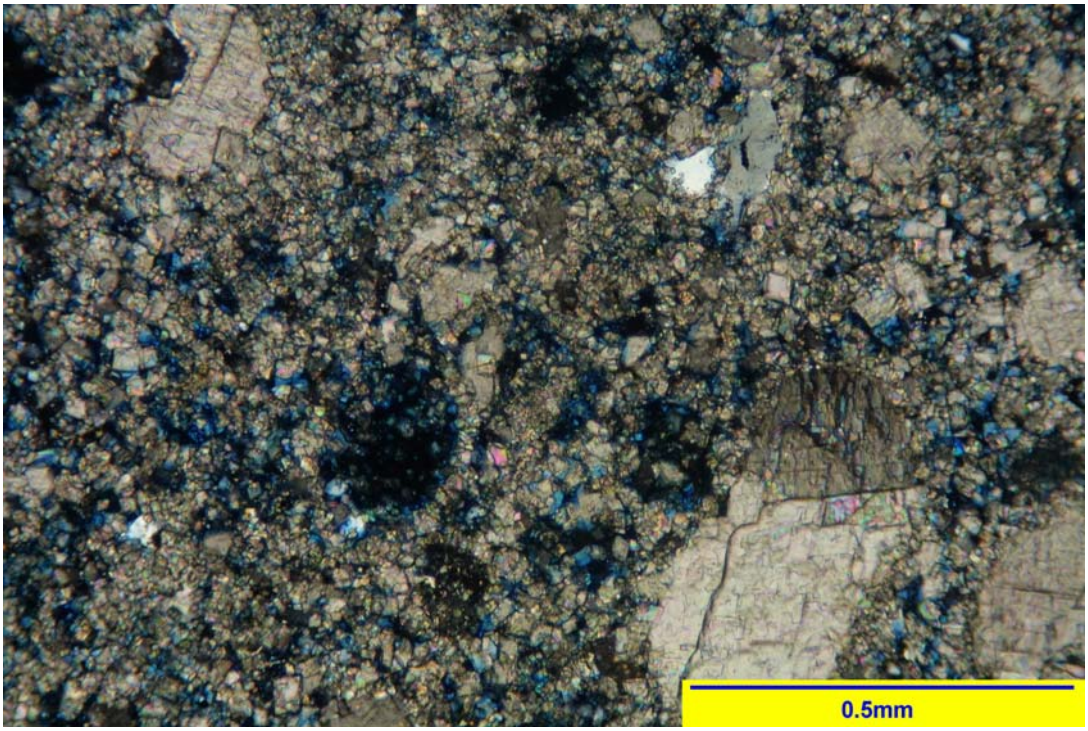

VIEW B : 90 x - Cross-polarized view from above center. Under cross-polarized view the blue epoxy shows as black.

PHOTOPLATE 15 - SCANNING ELECTRON MICROSCOPE PHOTOMICROGRAPHS

Big Lime Formation - 1396.20 ft. - (12.7%, 0.34mD)

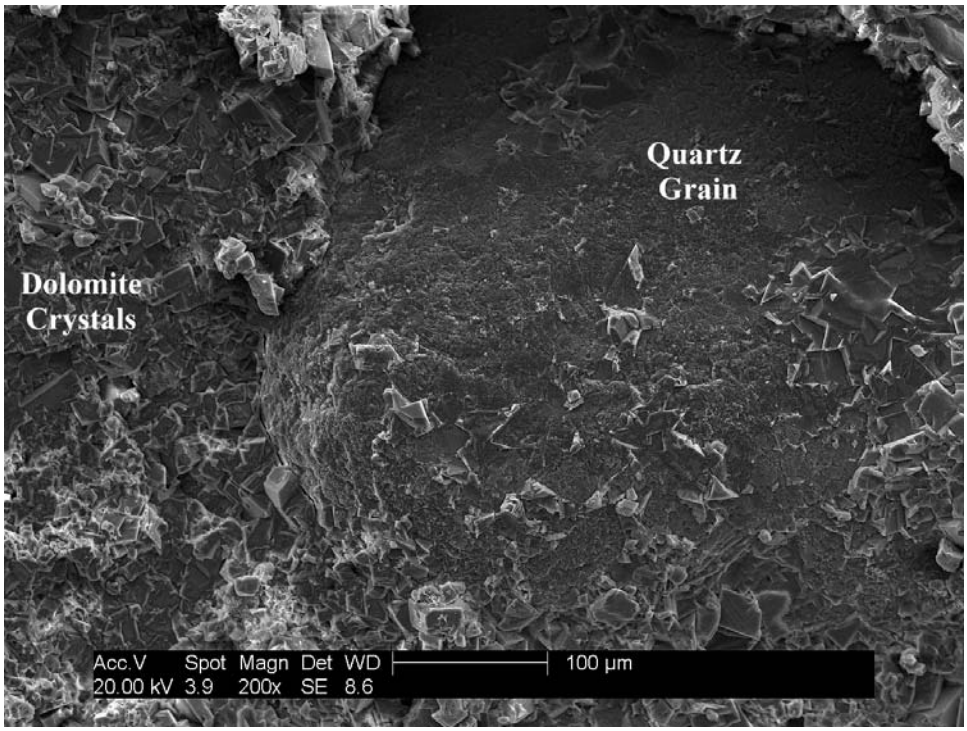

VIEW A : A large quartz grain takes up most of this view and rests in a matrix of Fe-rich dolomite crystals. Interparticle porosity is considered Fair in this zone.

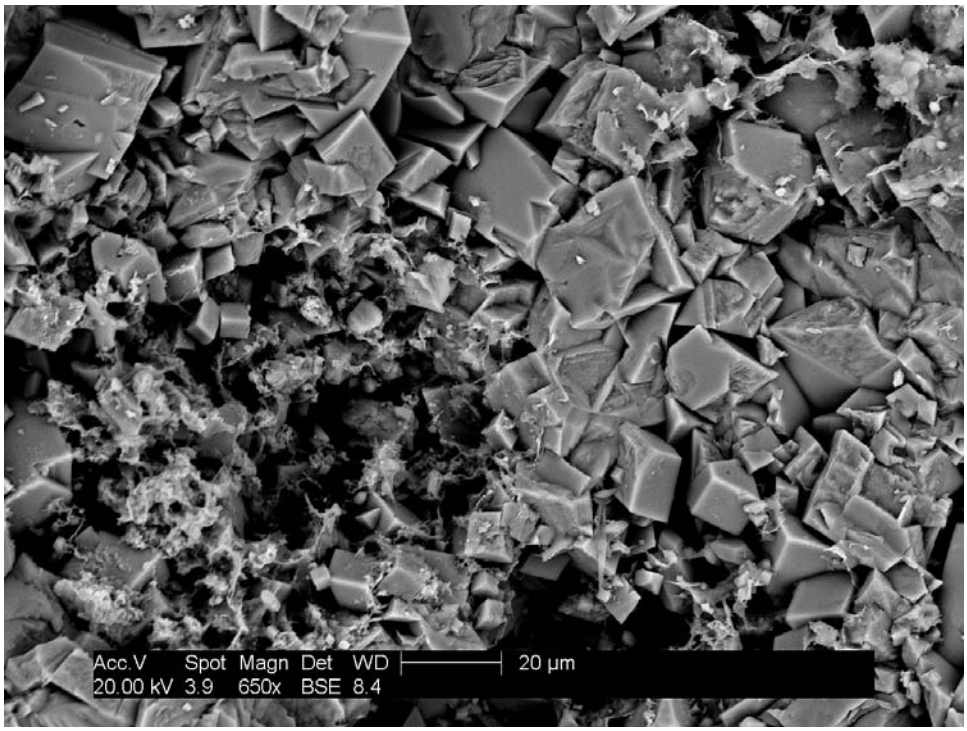

VIEW B : Illitic clay can be seen here bridging, otherwise open pore spaces between Fe-rich dolomite crystals. Fragile illitic clays can pose a threat to porosity by breaking free and brush-piling at pore throats during hydraulic fracturing, however the clay content in these samples was found only in trace amounts during XRD analysis indicating an insignificant portion of clay in these samples.

PHOTOPLATE 16 - THIN SECTION ANALYSIS PHOTOMICROGRAPHS

Big Lime Formation - 1396.20 ft. - (12.7%, 0.34mD)

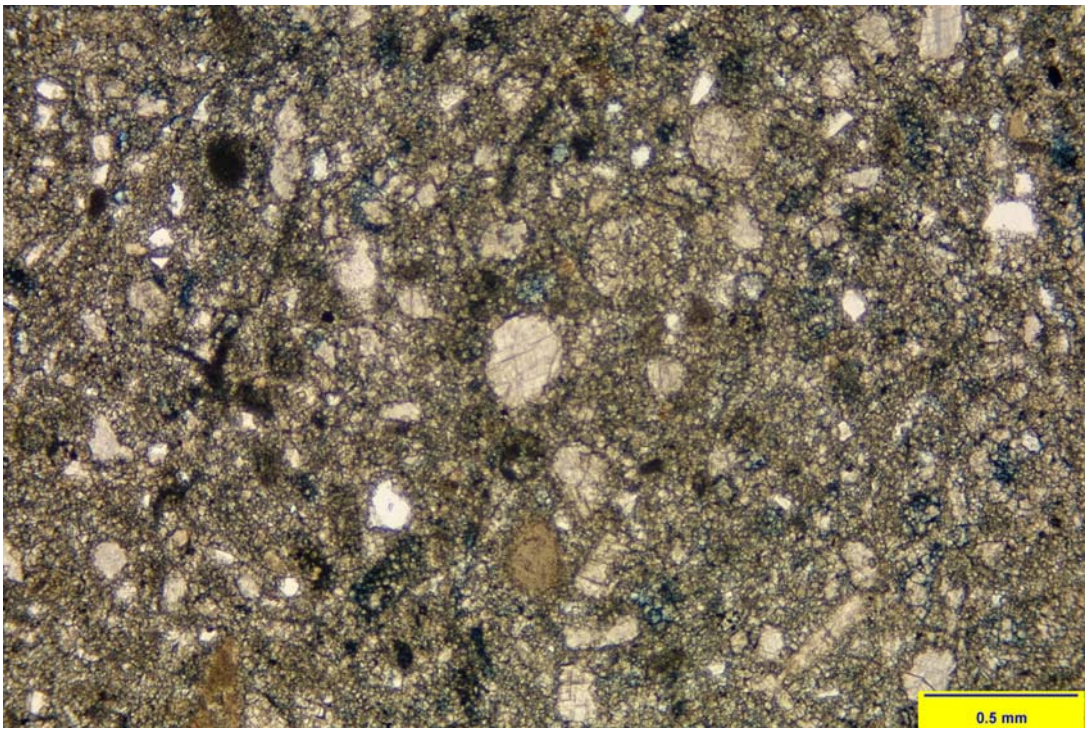

VIEW A : 40x - Generalized view showing a fine grained dolomite consisting of medium grained dolomite "pellets" and trace amounts of fine to medium grained, monocrystalline quartz.

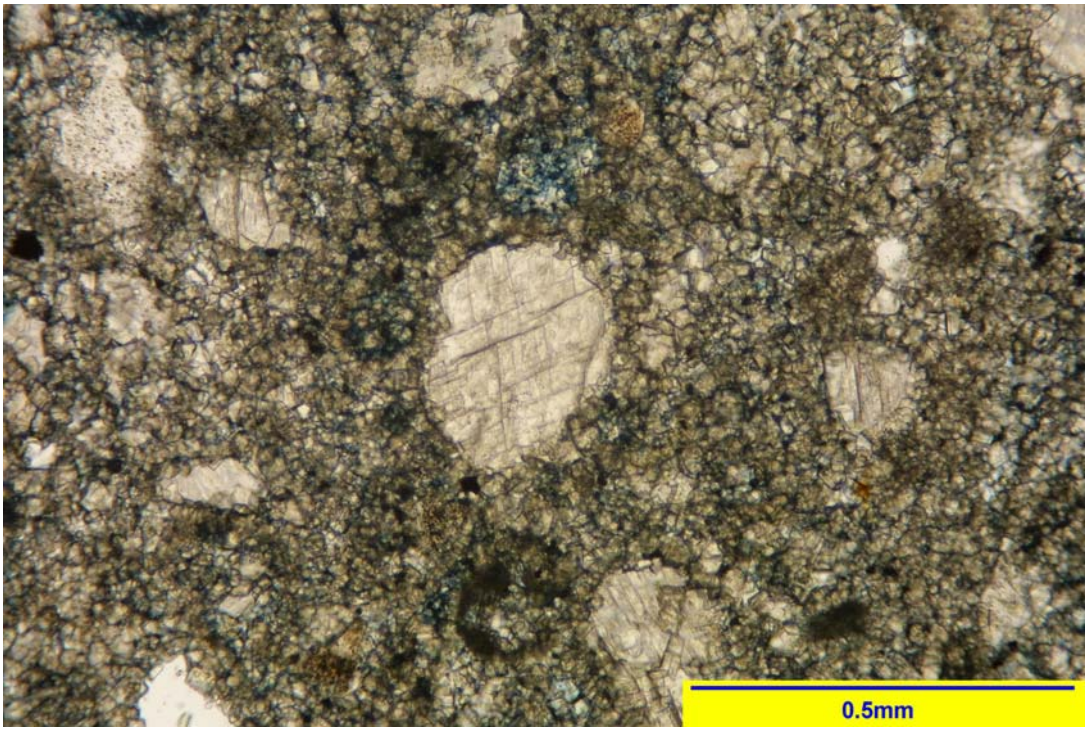

VIEW B : 90x - Close-up view from above center.

PHOTOPLATE 17 - SCANNING ELECTRON MICROSCOPE PHOTOMICROGRAPHS
Big Lime Formation - 1397.40 ft. - (14.8%, 0.70mD)

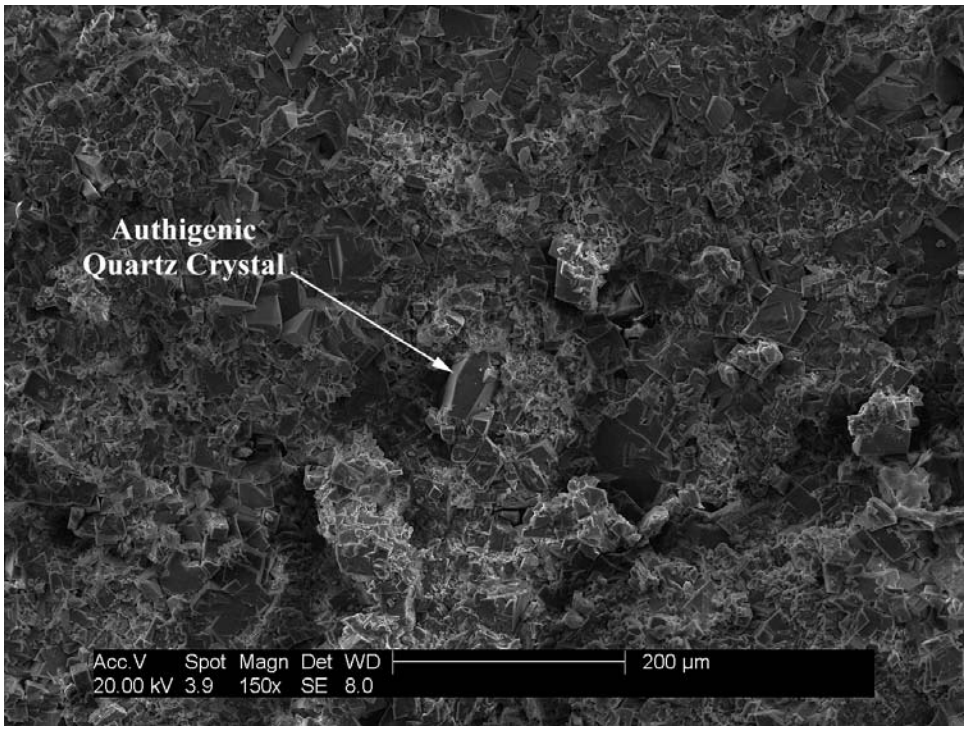

VIEW A : Interparticle porosity is Good in this zone with several large, open, interparticle pores scattered across this view.

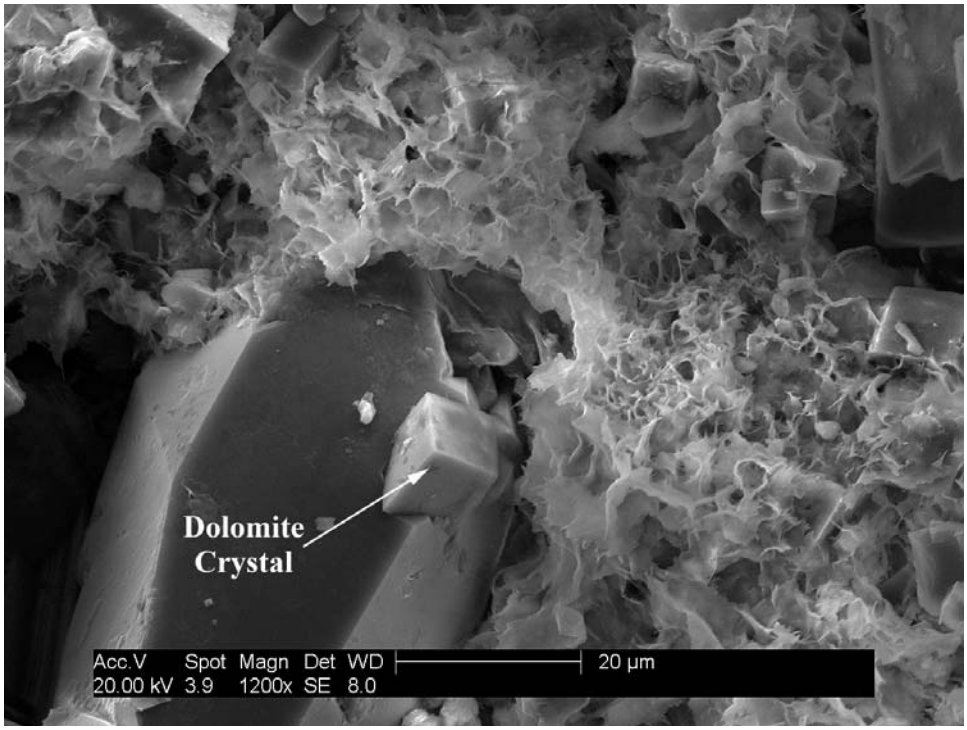

VIEW B : In this close-up view of the authigenic quartz crystal, from View A, a dolomite crystal can be seen embedded in the quartz. In this case the quartz grew into a void (or vug) in the dolomite, growing up around the preexisting dolomite crystal.

PHOTOPLATE 18 - THIN SECTION ANALYSIS PHOTOMICROGRAPHS

Big Lime Formation - 1397.40 ft. - (14.8%, 0.70mD)

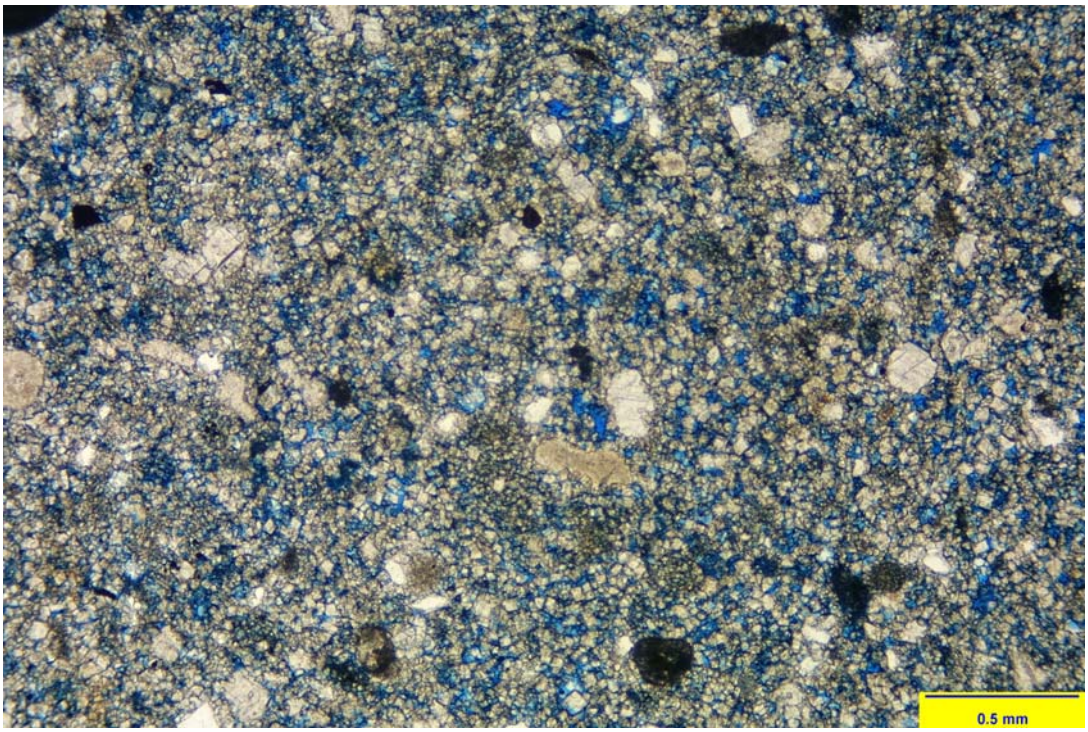

VIEW A : 40x - Generalized view showing a porous, fine to medium grained dolomite consisting of subhedral to euhedral, fine to medium dolomite with trace to minor amounts of medium grained, monocrystalline quartz.

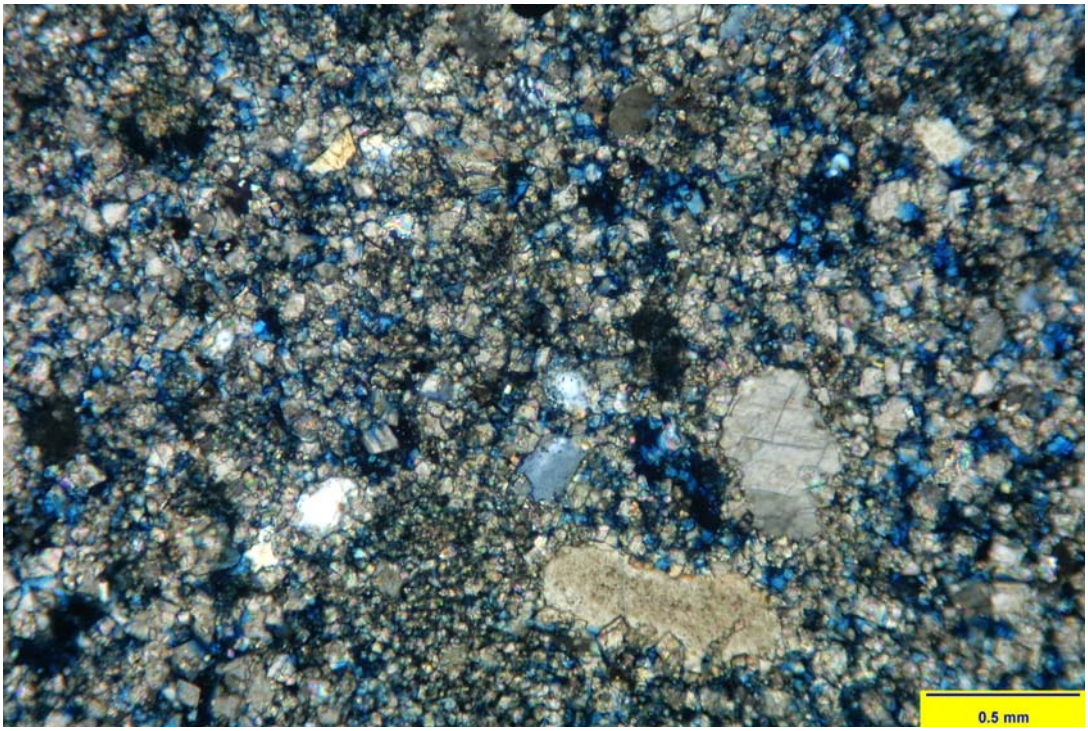

VIEW B : 90x - Cross-polarized view from center above.

PHOTOPLATE 19 - SCANNING ELECTRON MICROSCOPE PHOTOMICROGRAPHS

Big Lime Formation - 1402.60 ft. - (5.7%, 0.02mD)

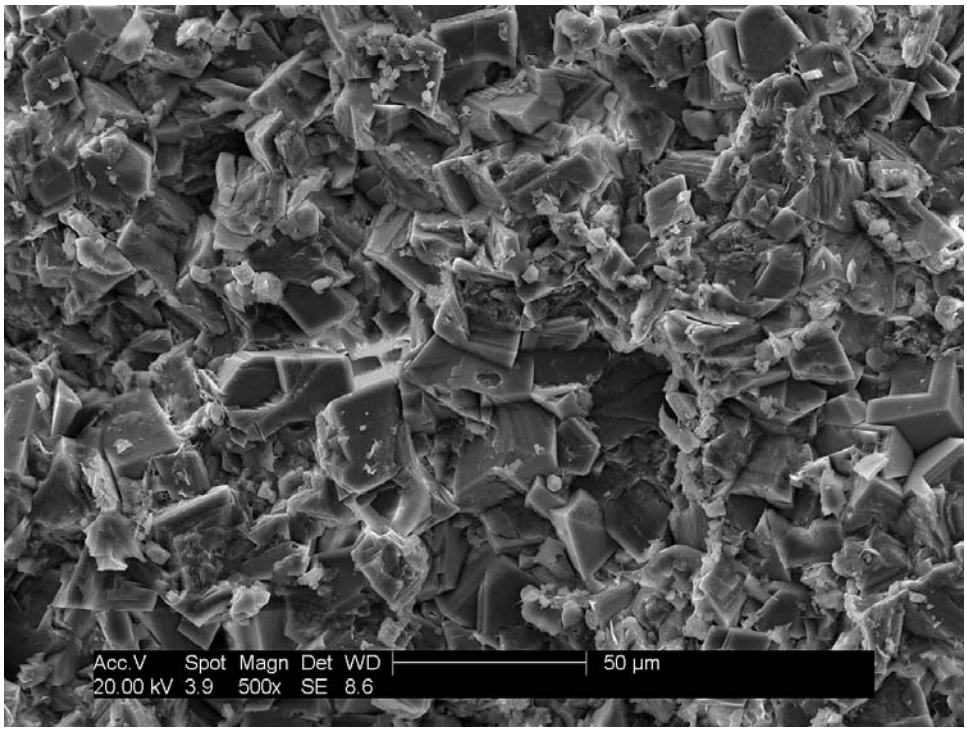

VIEW A : Interparticle porosity in this Fe-rich dolomite is considered Poor. Microporosity adds significantly to total porosity in this zone.

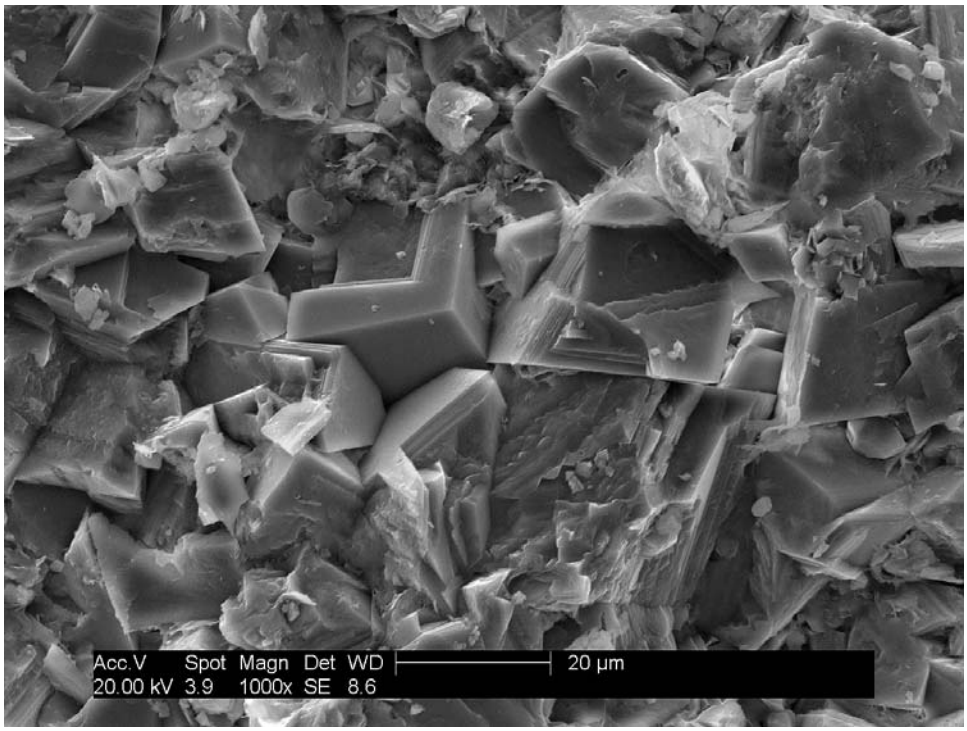

VIEW B : Close-up of dolomite crystals showing where microporosity exists between the crystals.

PHOTOPLATE 20 - THIN SECTION ANALYSIS PHOTOMICROGRAPHS

Big Lime Formation - 1402.60 ft. - (5.7%, 0.02mD)

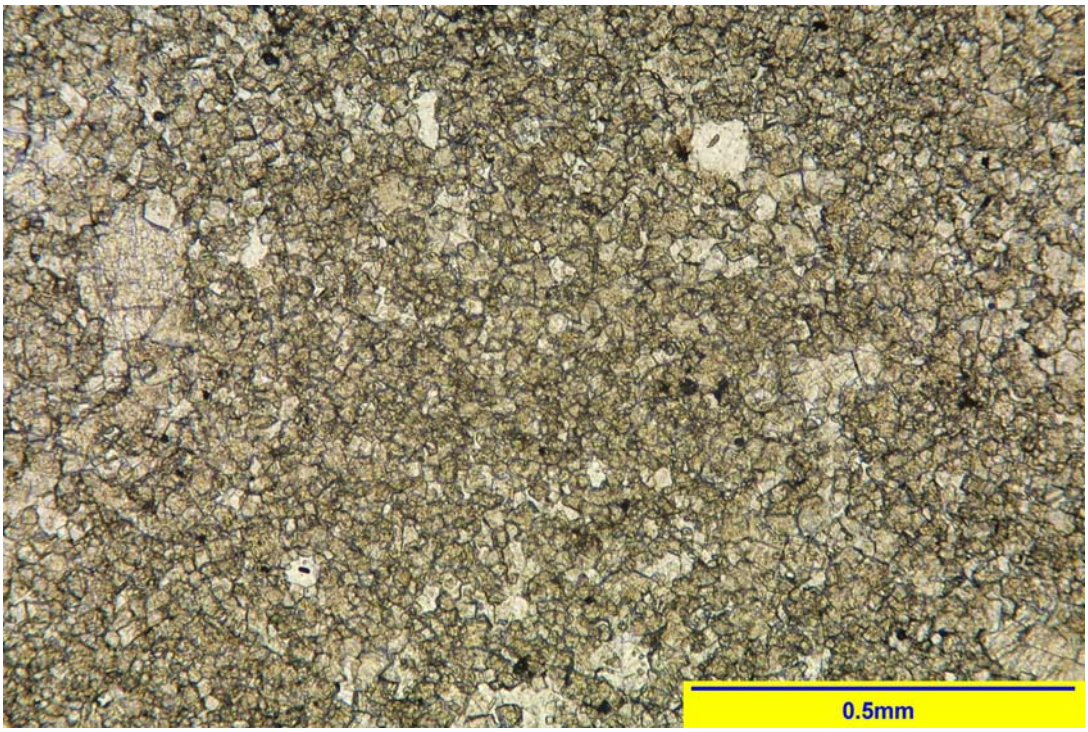

VIEW A : 90x - General view showing a very fine grained quartzose dolomite consisting of fine grained monocrystalline quartz in a fine grained dolomite matrix.

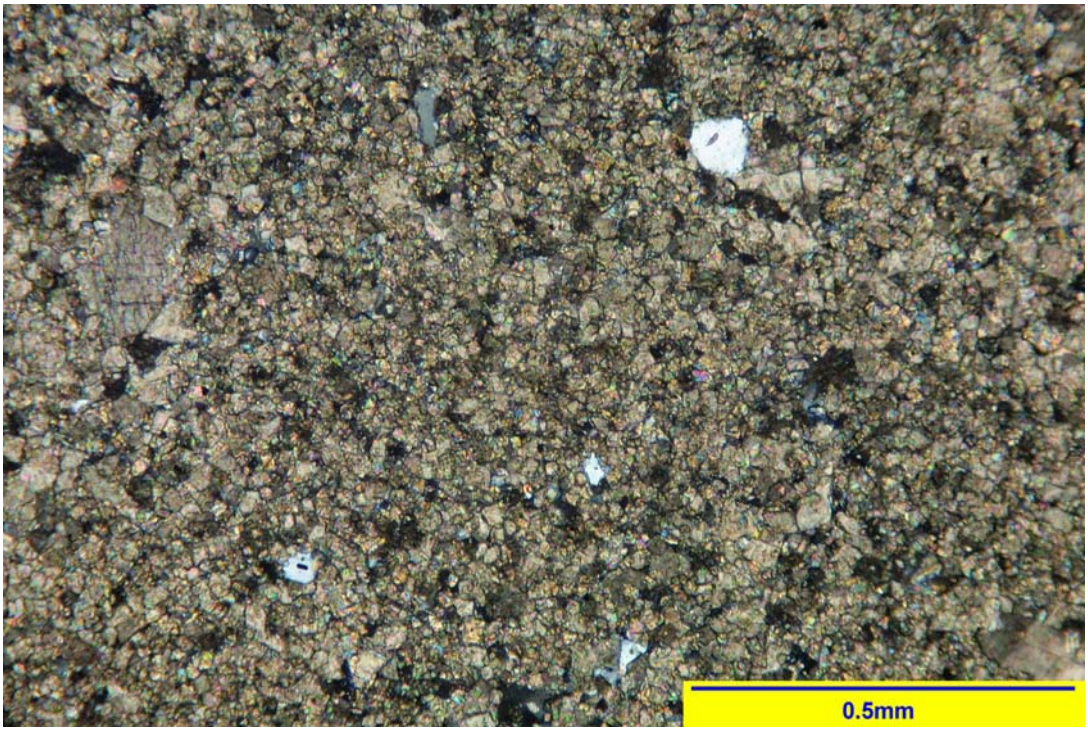

VIEW B : 90x - Cross-polarized view of View A. Note: No visible macro-porosity.

ANALYTICAL PROCEDURES:

Stereomicroscopy

Stereomicroscopy is a reflected light microscopy technique performed at relatively low magnifications, commonly 20X and 63X. This technique is used to assess rock textural parameters and to subsample large sample sets for other analyses such as scanning electron microscopy, thin section petrology, and X-ray diffraction.

Scanning Electron Microscopy/Energy Dispersive Spectrometry

Scanning electron microscopy/energy dispersive spectrometry (SEM/EDS) uses an electron beam generated in a vacuum chamber to image the sample. Samples are prepared by extracting volatile hydrocarbons and drying at low temperature. The cleaned and dried samples are subsequently sputter-coated with a 30 Angstrom thick layer of gold under vacuum. As the electron beam strikes the sample surface, topography sensitive secondary electrons are generated, collected in a detector, and computer imaged. X-rays are also generated while the sample is being scanned. The energy levels of these X-rays are characteristic of the elements from which they were generated. The X-ray energies are computer-imaged into an elemental (EDS) spectrum showing qualitative atomic composition of the sample. SEM/EDS techniques are used to provide both high and low magnification views of the sample with great depth of field, yielding interpretations of the interrelationships between grains, pore types, cements, and clays. SEM techniques are particularly useful in assessing the occurrence of clays within the pore network.

X-Ray Powder Diffraction

X-ray powder diffraction (XRD) is an analytical technique that bombards a finely-powdered rock sample with monochromatic Cuk" radiation and measures intensity of the scattered beam versus 2-theta angle of the instrument. These data are used in the Bragg equation to calculate d-spacings of the material(s) present. *Bulk XRD samples* are prepared by mechanically grinding the sample to a fine powder and back-packing the powder into a hollow-cavity sample mount. *Clay samples* are prepared by separating the clay-size fraction from the bulk sample, and depositing a slurry containing the "clays" on a glass slide. Additional treatments of clay samples by glycolating (to distinguish smectite and expandable mixed-layer clays) and heat treating (to discern kaolinite from chlorite) are performed as needed. XRD is used to provide semi-quantitative data on the relative abundances of bulk and clay minerals present in rock samples analyzed. Such percentages are often critical to stimulation treatment design.

Acid Solubility Testing

Acid solubility testing involves digestion of a finely-sieved sample in excess 15% hydrochloric acid (HCl) at reservoir temperature for approximately 1 hour. Following digestion, the remaining sample is dried in a convection oven before obtaining a final sample weight and calculating weight loss (solubility) as a percent of initial sample weight. If appropriate, the acid-soluble iron content of the sample is also measured.

Thin Section Petrography

Thin section petrography uses light transmitted through a thin (30 micron) section of rock to image the sample. Samples are prepared by injecting porosity with blue-dyed epoxy-resin under vacuum and pressure, attaching to a glass slide, and grinding to a final 30 micron thickness. Samples may be stained for rapid identification of calcite and/or potassium feldspar. Thin section petrology descriptions commonly include textural parameters such as grain size, sorting, and

roundness, cementation, and porosity types/relationships. Thin sections may also provide some limited data on clays in the sample.

Routine Core Analysis

Helium porosities (ϕ) were determined by the Boyle's Law technique using a combination of the sample's grain volume and bulk volume. Cleaned and dried core plugs of known weight and dimensions (bulk volume) were placed in a calibrated matrix cup. After expanding helium into the core plug to measure grain volume, the grain volume was subtracted from the bulk volume yielding porosity, reported as percent of bulk volume. Grain density was calculated as grain weight divided by grain volume and is reported in grams per cubic centimeter.

Gas permeability measured at ambient conditions is a specific permeability to gas (100% gas saturation). Cleaned and dried core plugs were inserted into rubber sleeves and placed in a core holder, where confining stress was applied to prevent gas bypass during permeability testing. Nitrogen gas was flowed through the plug until constant upstream and downstream pressures, and constant flow rate were obtained. Darcy's equation for laminar gas flow was used to calculate specific gas permeability.